

**Development of an Improved RF Band-Pass Filter
using CSRR Metamaterial Structures on an LCP Substrate**

by

Christopher Brent James

A thesis submitted to the Graduate Faculty of
Auburn University
in partial fulfillment of the
requirements for the Degree of
Master of Science in Electrical Engineering

Auburn, Alabama
May 10, 2015

Keywords: Metamaterial, CSRR, Band-Pass, Filter, HFSS, LCP

Approved by

Robert Dean, Chair, Associate Professor of Electrical and Computer Engineering
Lloyd S. Riggs, Professor of Electrical and Computer Engineering
Michael Baginski, Associate Professor of Electrical and Computer Engineering

Abstract

For over a decade, academic exploration into the emerging field of metamaterial technology has resulted in advancements in the design of myriad devices such as oscillators, antennas, transmission lines, superlenses, and filters. Unusual electromagnetic properties unique to metamaterial structures have also inspired new work in fields like cloaking technology and nanotechnology. Two such structures that are of interest to RF and microwave engineering applications are the split-ring resonator (SRR) and its dual, the complementary split-ring resonator (CSRR). An RF band-pass filter based on a previous work is designed using a microstrip transmission line on a substrate made of Liquid Crystal Polymer (LCP), a flexible material with desirable RF properties such as a low dielectric constant ϵ . This transmission line is made of copper and is coupled to a CSRR structure etched into a ground plane below the substrate. The band-pass frequency response is dependent on the physical dimensions of both the microstrip line and the CSRR structure. The proposed filter is designed as a unit cell with a single CSRR structure, and the S-parameters of the filter are simulated for frequencies ranging from 1 GHz to 10 GHz. Both the design and the simulation of the filter are done using HFSS, a commercial simulation tool by ANSYS that uses finite element method (FEM) techniques to solve electromagnetic structures. With an emphasis on improving the upper-band performance, this work seeks to design a compact RF band-pass filter using metamaterial technology that can be applied to non-planar surfaces.

Acknowledgments

The author would like to take this opportunity to recognize those who, through financial, intellectual, or emotional means, provided the necessary support to make this work possible: the American Society for Engineering Education and the SMART program for tuition and stipend support; his advisor Dr. Robert Dean, as well as committee members Dr. Lloyd Riggs and Dr. Michael Baginski, for their knowledge, patience, and professional example; Dr. Stu Wentworth, Dr. John Hung, Dr. Shumin Wang, and others in the Auburn University Department of Electrical and Computer Engineering for their willingness provide technical guidance and constructive criticism; Dr. Guy Beckwith, Mr. Chris Henderson, and Ms. Vickie Lundy for their inspiration and academic influence on his education and career decisions; Udarius Blair, Byron Caudle, William Little, and Christopher Wilson for their academic and technical advice; his parents, Brent and Beth James, as well as the rest of his family and friends for their consistent and unwavering support; and his wife, Alison, for always believing.

Table of Contents

Abstract.....	ii
Acknowledgments.....	iii
Table of Figures	v
List of Abbreviations	viii
Chapter 1: Introduction.....	1
Chapter 2: Metamaterial Theory.....	4
Chapter 3: Microwave Filter Theory	15
Chapter 4: Metamaterial Filters	26
Chapter 5: HFSS	37
Chapter 6: Improved BPF Design.....	50
Chapter 7: Conclusion.....	59
Chapter 8: Future Work	60
Bibliography	61

Table of Figures

Figure 2-1.....	6
Figure 2-2.....	6
Figure 2-3.....	7
Figure 2-4.....	8
Figure 2-5.....	9
Figure 2-6.....	10
Figure 2-7.....	11
Figure 2-8.....	12
Figure 2-9.....	13
Figure 2-10.....	13
Figure 3-1.....	16
Figure 3-2.....	17
Figure 3-3.....	18
Figure 3-4.....	19
Figure 3-5.....	20
Figure 3-6.....	21
Figure 3-7.....	21
Figure 3-8.....	23
Figure 3-9.....	25
Figure 4-1.....	27
Figure 4-2.....	28
Figure 4-3.....	29

Figure 4-4.....	30
Figure 4-5.....	31
Figure 4-6.....	32
Figure 4-7.....	33
Figure 4-8.....	34
Figure 4-9.....	34
Figure 4-10.....	35
Figure 4-11.....	35
Figure 4-12.....	36
Figure 5-1.....	38
Figure 5-2.....	39
Figure 5-3.....	40
Figure 5-4.....	41
Figure 5-5.....	41
Figure 5-6.....	42
Figure 5-7.....	43
Figure 5-8.....	43
Figure 5-9.....	44
Figure 5-10.....	45
Figure 5-11.....	45
Figure 5-12.....	46
Figure 5-13.....	47
Figure 5-14.....	48

Figure 5-15.....	49
Figure 6-1.....	50
Figure 6-2.....	51
Figure 6-3.....	52
Figure 6-4.....	53
Figure 6-5.....	54
Figure 6-6.....	55
Figure 6-7.....	56
Figure 6-8.....	56
Figure 6-9.....	57
Figure 6-10.....	58

List of Abbreviations

RF	Radio frequency
LHM	Left-handed medium
DNG	Double-negative
LCP	Liquid crystal polymer
SRR	Split-ring resonator
CSRR	Complementary split-ring resonator
CPW	Coplanar waveguide
CRLH	Composite right/left-handed
MEMS	Microelectromechanical systems
SAW	Surface acoustic wave
BAW	Bulk acoustic wave
LPF	Low-pass filter
HPF	High-pass filter
BSF	Band-stop filter
BPF	Band-pass filter
FEM	Finite element method

Chapter 1

Introduction

Influenced by the theoretical foundation established by Veselago in 1967, the works of Smith and Pendry near the beginning of the 21st century made possible the science of metamaterials [1] [2] [3]. These man-made structures, capable of unusual electromagnetic behavior not found in nature, have made possible novel approaches to the design of well-known electronic devices such as antennas, oscillators, lenses, and filters [4] [5] [6] [7]. Additionally, the advancement of metamaterial theory has opened doors for research in fields such as superlenses and cloaking technology.

Contrary to the name, metamaterials are actually not conventional materials, in the sense that they are not novel or synthetic substances. Rather, a metamaterial object is generally composed of periodic arrays of small artificial structures called unit cells made from dielectric materials, plastics, metals, and other commonly-used materials that have been engineered into specific structures or shapes. The properties and arrangement of these unit cells are what give the metamaterial its unique traits. In this sense, a metamaterial device can be considered analogous to matter, where its inherent properties are determined by the combination of smaller “building blocks” of different elements. In the case of matter, these properties are determined by the amount and arrangement of the atoms in the material and the types of bonds that exist between them; in the case of a metamaterial, its properties are determined by the physical dimensions of the unit cells that compose the device as well as the electromagnetic coupling mechanisms that enable its operation.

Since the early 2000s, the most common topic in metamaterials research is the concept of negative index metamaterials, also known as left-handed media (LHM) or double negative (DNG)

metamaterials—that is, metamaterials where the refractive index n is negative over a certain frequency range. This effect emerges from unusual behavior of the device’s relative permittivity and relative permeability—two properties that govern the way matter interacts with electromagnetic fields. By definition,

$$n = \sqrt{\varepsilon\mu} \quad (1.1)$$

where ε is the effective permittivity and μ is the effective permeability. Permittivity is the measure of a material’s interaction with electric fields in Farads/meter while permeability is the measure of interaction with magnetic fields in Henries/meter. These characteristics are seen in the constitutive relations with regard to Maxwell’s equations by

$$\vec{D} = \varepsilon\vec{E} \quad (1.2)$$

$$\vec{B} = \mu\vec{H} \quad (1.3)$$

When nearing the resonant frequency, the mathematical values of relative permittivity and relative permeability in these metamaterials become less than 0. This requires (1.1) be rewritten as

$$n = \pm\sqrt{\varepsilon\mu} \quad (1.4)$$

which allows a negative index of refraction without mathematical contradiction. This can result in backward propagation of traveling waves and negative wave impedance η , which makes designing metamaterial filters possible.

Metamaterial filters in the RF range are of particular interest due to their compact size and ease of design and fabrication. The difference between a “normal” microstrip filter and an RF metamaterial filter, for example, is little more than the extra work of etching rings into the filter’s

ground plane. Since metamaterials devices are composed of unit cells, high order filters can easily be fabricated using simple periodic arrangements of these structures. Also, since the frequency response is dependent upon the physical dimensions of the device and its components, factors like center frequency and bandwidth can be easily tuned by simply modifying the length, width, and height of the signal line and the metamaterial shapes. In the case of metamaterial filters, the filter type (low-pass, high-pass, band-pass, band-stop) can also be changed by adding or removing etched gaps and shunt stubs in the signal line.

The applications of negative-index metamaterials range from novel circuits for RF communication to potentially RF cloaking devices and everything in between. Even though the field of metamaterial technology has only recently become a practical reality, the interest and work in the field so far show the possibilities of continued exploration into novel designs of these devices.

Chapter 2

Metamaterial Theory

In his seminal work on substances with a negative refractive index, Veselago shows the relationship between the frequency of a wave ω and its wave vector k in an isotropic medium by presenting the dispersion equation

$$k^2 = \frac{\omega^2}{c^2} n^2 \quad (2.1)$$

where the square of the refractive index in (2.1) is given by

$$n^2 = \epsilon\mu \quad (2.2)$$

It quickly becomes apparent that simultaneously changing the sign of both ϵ and μ to be negative has no mathematical effect on the index of refraction. Due to the fact that before this time no negative-index materials had been observed, Veselago proposed three possible outcomes: one, changing the sign of both permittivity and permeability of a material would have no effect on the object since the index of refraction would mathematically be unchanged; two, this situation would violate some law of nature and a material with these properties could not exist; or three, that some substances with simultaneously negative ϵ and μ could exist and exhibit properties different from substances with positive ϵ and μ .

Veselago found that these theoretical negative-index substances were in fact capable of producing strange effects when the implications of negative ϵ and μ were further investigated separately. By analyzing the constitutive relations

$$\vec{B} = \mu\vec{H} \quad (2.3)$$

$$\vec{D} = \epsilon\vec{E} \quad (2.4)$$

Veselago found that, under the condition of $\varepsilon < 0$ and $\mu < 0$, \vec{E} , \vec{H} , and \vec{k} form a “left-handed” set of vectors where the directions of the Poynting vector \vec{P} and the wave vector \vec{k} are in opposite directions. This leads to a material with negative group velocity which Veselago named a “left-handed substance.” Effects that follow from this property include a reversal of the Doppler effect, where an increase or decrease in frequency at the receiver will be the opposite of what it would be in the usual “right-handed” case.

Another interesting phenomenon arises when the boundary conditions between two media are considered. To satisfy the tangential and normal components of the \vec{E} and \vec{H} fields at the boundary, the following equations must hold true:

$$\vec{E}_{t_1} = \vec{E}_{t_2} \quad \vec{H}_{t_1} = \vec{H}_{t_2} \quad (2.5)$$

$$\varepsilon_1 \vec{E}_{n_1} = \varepsilon_2 \vec{E}_{n_2} \quad \mu_1 \vec{H}_{n_1} = \mu_2 \vec{H}_{n_2} \quad (2.6)$$

It can be seen, then, that the signs of the normal components of \vec{E} and \vec{H} can be negative under the appropriate circumstances, leading to a change in the direction of the normal component of the field. Considering Snell’s Law

$$n_{12} = \frac{\sqrt{\varepsilon_2 \mu_2}}{\sqrt{\varepsilon_1 \mu_1}} \quad (2.7)$$

leads to a situation where a ray traveling from a right-handed medium to a left-handed medium can experience unusual refraction behavior as shown in Figure 2-1. Note that the ray is refracted at a negative angle with respect to the normal and that its direction of propagation is back to the inside of the shaded region. This unusual trajectory would be reexamined later as part of the first modern realization of negative-index materials.

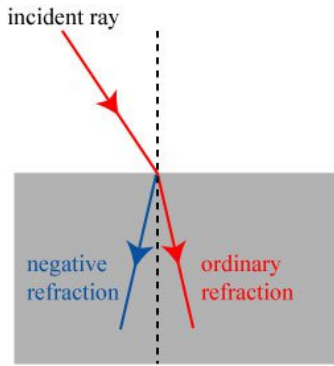


Figure 2-1: Wave refraction of an incident wave in the double-negative case (left) and a normal case. [8]

Near the turn of the century, Veselgo’s hypothesis of negative-index materials was realized in the work of John Pendry [3]. Pendry proposed a “super lens,” a device that would be matched to free space by the reversal of the phase shift of light as it moves away from a source, effectively having perfect focus. An illustration of light traveling through the theoretical lens is given below in Figure 2-2.

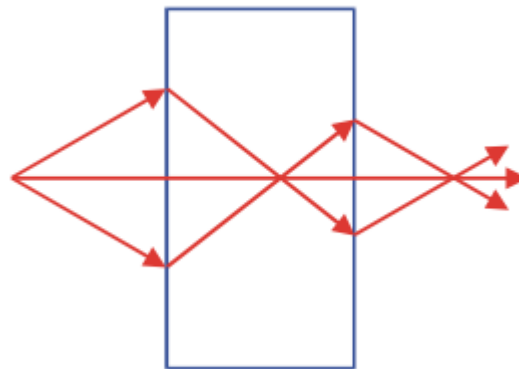


Figure 2-2: The path of a ray through a negative-index material is shown. The ray is bent at a negative angle which forces it to converge back to a point. [9]

Note that the ray in the figure enters the slab and then bends at a negative angle back towards the normal then bends back to a point upon exiting the slab. By tuning this material correctly, a perfect

match can be made between free space and the slab, resulting in what Pendry called a “perfect lens.”

This device would require a negative index of refraction, and therefore negative values of permeability and permittivity according to Equation 2.2. Previous work by Pendry and others had already established that periodic arrays of small sub-wavelength structures could yield negative permeability or permittivity, but an element showing simultaneously negative parameters—a true negative-index material—had not yet been presented [9] [10]. Pendry showed that infinitely long wires in a cube lattice structure could result in a negative ϵ_{eff} , and later he followed this work by demonstrating negative μ_{eff} through thin sheets of metal cut into split ring shapes in a three-dimensional array.

Smith and others at UCSD combined the two by experimentally demonstrating negative-index behavior capable of backwards wave propagation using conducting split-ring resonators (SRRs) in what were named “metamaterials.” [11] By spacing these conducting elements at a distance much less than a wavelength apart in periodic arrays, a medium was created that had both negative permittivity and negative permeability and therefore a negative index of refraction. An early example of a metamaterial composed of split-ring resonators is shown in Figure 2-3.

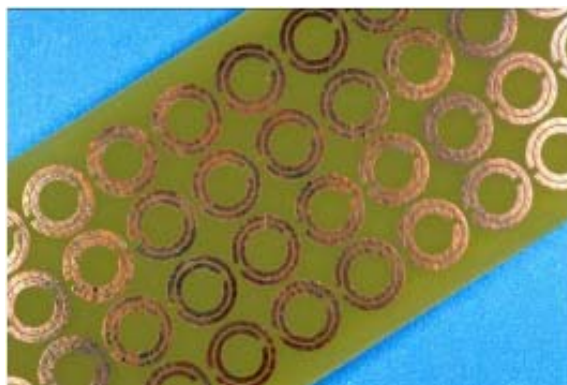


Figure 2-3: An early example of a metamaterial structure composed of split-ring resonator elements arranged in a periodic array. [12]

Using this structure, the analogy of a metamaterial to a conventional material can be made. While the properties of conventional materials are dictated by chemical composition (the arrangement of individual atoms and molecules and the properties associated with their chemical bonds), metamaterial properties are derived from periodic elements ranging in size from nanometers to millimeters (and therefore made up of several atoms) that compose the larger structure. That is, each SRR in the metamaterial acts as a single atom as shown below in Figure 2-4.

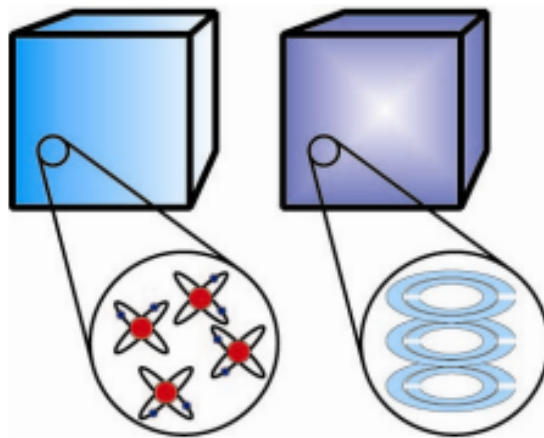


Figure 2-4: Split-ring resonator structures in metamaterials are like atoms in conventional materials, acting as small “building blocks” and giving the larger structure its unique properties. [12]

The SRR is a relatively simple structure made of two concentric metal rings, each with a gap on opposing sides of the element. One ring sits inside of another with a set separation distance between the outer radius of the smaller ring and the inner radius of the larger ring. This element is usually much smaller than a wavelength in size, and a metamaterial device can have as many as hundreds of these elements placed at small periodic intervals. The physical dimensions of the rings and gaps in the SRR are relevant to the properties of the resonator, and any changes in ring width, gap width, ring spacing, or ring diameter all will affect the frequency response in some significant

way. The SRR can be modeled as an LC resonator excited by an external magnetic flux. An illustration of some of the relevant ring dimensions and the equivalent circuit model are shown below in Figure 2-5.

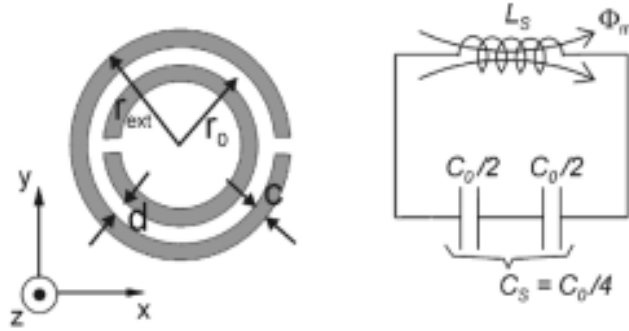


Figure 2-5: Left: Top view of a split-ring resonator (SRR). Right: Equivalent circuit model of an SRR. The SRR can be modeled as an LC resonator. [13]

In the figure, C_o denotes the capacitance between the two rings and is given by

$$C_o = 2\pi r_o C_{pul} \quad (2.8)$$

where C_{pul} is the per-unit length total capacitance between the rings and r_o is the averaged radius between the two rings. The series capacitance and inductance of the rings in the SRR are given by

$$C_s = C_o/4 \quad (2.9)$$

and L_s can be approximated as the inductance of a single ring of radius r_o . The resonant frequency of the SRR is given by

$$f_o = \frac{1}{2\pi\sqrt{L_s C_s}} \quad (2.10)$$

In the time since Smith demonstrated the SRR, several other resonating structures have been proposed including square split-ring resonators, H-shaped resonators, and spiral resonators [14] [15] [16]. In addition to new types of resonating structures, a physical dual of the SRR has

been demonstrated, called the complementary split-ring resonator (CSRR) [17]. Whereas the SRR is usually made of some metal on top of (or etched into the top of) some substrate and incorporated into the signal line, the CSRR is instead a negative image of the SRR and is etched into the metal ground plane underneath the substrate and signal line. The SRR is excited by an external axial magnetic flux while the CSRR is excited by an axial electric field. Just as above, the CSRR can be modeled as an LC resonator following the principle of duality by replacing the shunt inductance with series capacitance and the series capacitors with shunt inductors as shown in Figure 2-6 below.

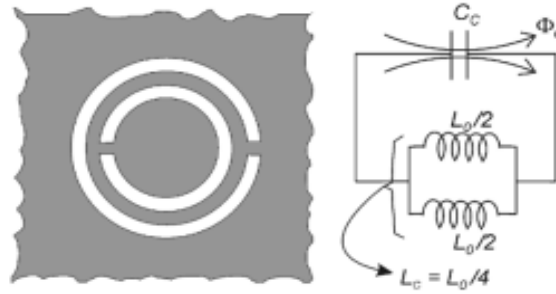


Figure 2-6: Left: Top view of a complementary split-ring resonator (CSRR).

Right: Equivalent circuit model of a CSRR. [13]

where the parameters of the equivalent circuit model are found similar to above. L_0 is given by

$$L_0 = 2\pi r_o L_{pul} \quad (2.8)$$

where L_{pul} is the per-unit length inductance. The series capacitance and inductance of the rings in the CSRR are given by

$$L_c = L_0/4 \quad (2.9)$$

and C_c is the capacitance of a disk of radius $r_o - c/2$. The resonant frequency of the CSRR is given by

$$f_o = \frac{1}{2\pi\sqrt{L_c C_c}} \quad (2.10)$$

In order to realize left-handed behavior in electronic applications and create practical negative-index media, it has been shown that these SRR and CSRR structures can be attached to a host transmission line made of either coplanar waveguide (CPW) or microstrip, respectively [18] [19] [20]. SRR host lines are loaded with shunt inductive elements while CSRR host lines are loaded with series capacitance elements. In the case of CPW, SRRs can be etched into the back substrate beneath the shunt strips of line; similarly, in the case of microstrip, CSRRs can be etched into the ground plane below the series gaps in the line. Examples of an SRR-loaded CPW and a CSRR-loaded microstrip line are shown below in Figure 2-7.

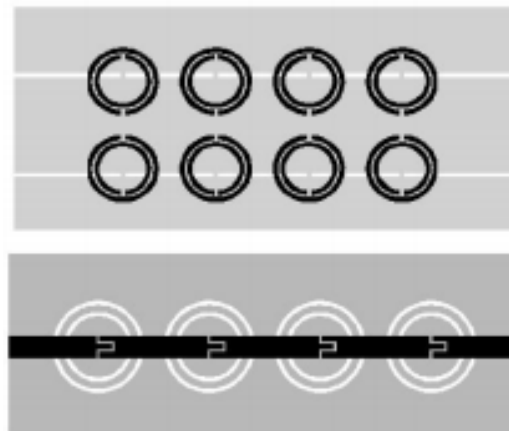


Figure 2-7: Top: SRR-loaded coplanar waveguide transmission line, where SRRs are located under shunt strips of line. Bottom: CSRR-loaded microstrip line, where CSRRs are located under the series gaps. [18]

While the electromagnetic mechanisms at work in these two types of resonating structures are different, it has been shown that the behavior of the transmission lines to which they are applied is similar because of the principle of duality [20]. These lines exhibit what is called a composite right/left handed (CRLH) behavior, where backward wave propagation is observed at relatively low frequencies. At these low frequencies, the reactive elements—the SRRs and/or CSRRs—dominate the frequency response. As frequency increases, the loading elements—the shunt inductance and/or series capacitance—begin to dominate line behavior.

A circuit model of a simple CRLH line is given below in Figure 2-8.

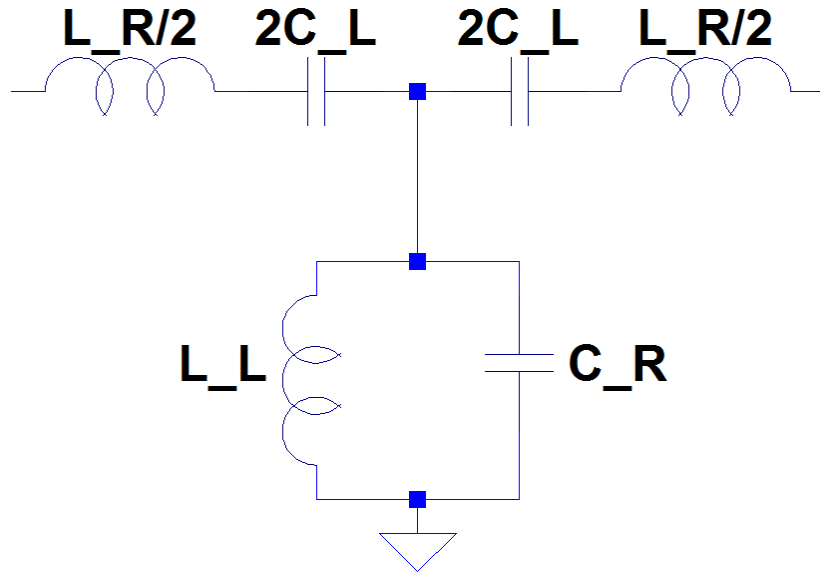


Figure 2-8: Lumped element equivalent circuit model of a CRLH transmission line.

In the lumped element model, C_L and L_L represent the capacitance and inductance of the transmission line's reactive elements and C_R and L_R are the per-section capacitance and inductance of the host line. Using this model, the negative effective permittivity and permeability can be realized using the following equations:

$$\epsilon_{eff} = \frac{C_R}{l} - \frac{1}{\omega^2 L_L l} \quad (2.11)$$

$$\mu_{eff} = \frac{L_R}{l} - \frac{1}{\omega^2 C_L l} \quad (2.12)$$

It can be seen, then, that at low frequencies where the negative component dominates the above two equations, negative effective permittivity and permeability are possible. The same is true when low values of C_L and L_L are present. As the frequency increases, however, the positive components dominate the equations, resulting in the CRLH line having “normal” right-handed behavior.

The lumped element equivalent circuit model for the SRR-loaded transmission line is given below in Figure 2-8 and the CSRR-loaded line is shown in Figure 2-9.

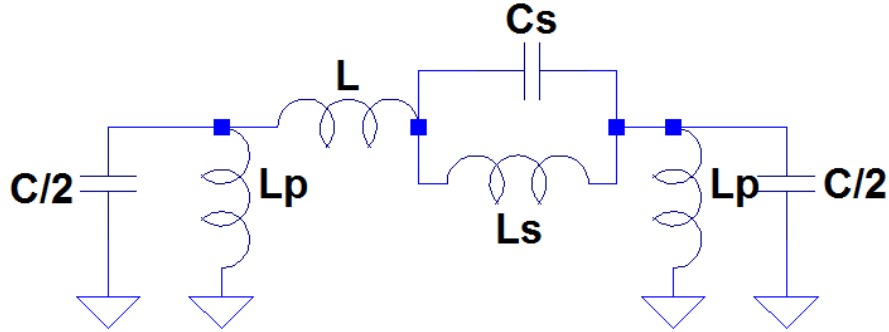


Figure 2-9: Lumped element equivalent circuit model of an SRR-loaded CPW.

In the SRR model, L and C model the inherent inductance and capacitance of the CPW line. L_p models the inductance of the shunt strips connected to the CPW, and L_s and C_s model the inductance and capacitance of the metamaterial rings.

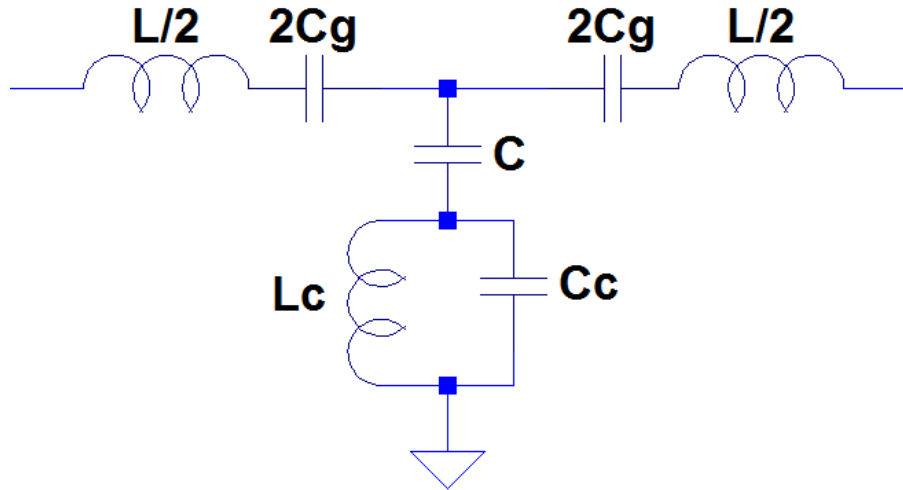


Figure 2-10: Lumped element equivalent circuit model of a CSRR-loaded microstrip line.

In the CSRR model, L and C model inductance and the capacitance of the microstrip line and C_g models the capacitance of the gaps in the line. L_c and C_c model the inductance and capacitance of the rings in the CSRR structure.

The presence of metamaterial resonators in CPW and microstrip transmission lines results in interesting and practically useful effects. While metamaterial transmission lines are capable of negative permittivity and permeability, this effect only occurs under certain conditions that are dependent on the dimensions of the device. Additions to the signal line in the form of shunt strips or etched gaps cause the structure to behave as a negative-index material up to its plasma frequency. As long as the plasma frequency is greater than the resonant frequency of the SRRs or CSRRs, the device will act as a negative-index metamaterial over the frequency range defined by

$$f_{L_s} = \frac{1}{2\pi} \sqrt{\frac{1}{C_s(2L+8L_p)} + \frac{1}{L_s C_s}} \quad (2.13)$$

$$f_{H_s} = \frac{1}{2\pi} \sqrt{\frac{1}{2C_s L} + \frac{1}{L_s C_s}} \quad (2.14)$$

$$f_{L_c} = \frac{1}{2\pi} \frac{1}{\sqrt{L_c \left(C_c + \frac{4}{\frac{1}{C_g} + C} \right)}} \quad (2.15)$$

$$f_{H_c} = \frac{1}{2\pi \sqrt{L_c C_c}} \quad (2.16)$$

where f_{L_s} and f_{H_s} define the left-handed bandwidth for the SRR case and f_{L_c} and f_{H_c} define the left-handed bandwidth for the CSRR case [21]. The model elements for all variable parameters are given on the previous page in Figure 2-8 and Figure 2-9. It is over this left-handed bandwidth that backward wave propagation occurs. Since the values in the lumped element model depend on the physical dimensions of the device, it can be concluded that these transmission lines can be easily tuned to different frequency ranges by simply changing the lengths, widths, height, and radii of the lines, stubs, and gaps that make up the device.

Chapter 3

Microwave Filter Theory

To understand the design and analysis of a metamaterial filter, it is beneficial to review some basic but relevant aspects of microwave filter theory. Simply put, a filter is a device that removes undesired frequency components of a signal while allowing other frequency components. More specifically, a microwave filter is a two-port electronic device that attenuates unwanted frequency components of a certain electrical signal and allows transmission of desired frequency components of the signal specifically in the microwave region of the electromagnetic spectrum (~300MHz to 300GHz). The ability to filter out unwanted electrical signals has applications in several areas of engineering, including wireless communication and signal processing. In the design of microwave filters, some important factors include cost, manufacturing and fabrication difficulty, physical size, and ease of integration with other technologies. Filters can be divided into three types: active (requiring an external power source), passive (requiring no external power source), and hybrid. In addition, filters can be classified based on their frequency response: low-pass, high-pass, band-stop, and band-pass, all of which will be explained in this chapter.

A microwave filter can be represented as a two-port network, a circuit with two pairs of terminals that connect the network to external circuitry. These pairs of terminals are called ports under the condition that the current entering one terminal is equal to the current exiting the second terminal. Modeling a filter as a two-port network simplifies the analysis of the device by isolating it from the rest of the circuit, leaving the device to be viewed as a “black box.” Two-port networks can be analyzed using several different measures of performance—scattering (S) parameters, ABCD parameters, and open-circuit impedance (Z) parameters, among others. In this work, S-parameters of a metamaterial filter will be analyzed. The four S-parameters are as follows: the

input reflection coefficient S_{11} , the output reflection coefficient S_{22} , the forward transmission gain S_{21} , and the reverse transmission gain S_{12} . S_{11} is also known as the return loss, and it refers to the measure of loss of port 1 where port 2 is terminated by a matched load. S_{21} is also known as the insertion loss, and it refers to the measure of loss from port 1 to port 2 when both ports are using the same reference impedance. S_{22} and S_{12} are similar to S_{11} and S_{21} , respectively, for port 2 instead of port 1. All four parameters are measured in decibels (dB). An example of a simple two-port network is shown below in Figure 3-1.

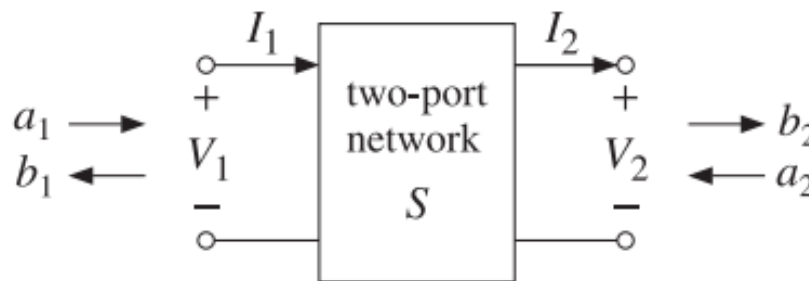


Figure 3-1: Example of a two-port network. [22]

When analyzing the performance of microwave filters or other frequency-dependent devices, the S-parameters are commonly presented as plots on a graph of magnitude in dB vs. frequency in Hz with the parameters S_{11} and S_{21} being the most common inclusions. In the case of microwave filters, S_{11} represents how much power is reflected from the input terminal, and S_{21} represents how much power is transferred through the device. For example, an S_{21} at a certain frequency of -10dB means that for every 1 Watt delivered to port 1, 0.1 Watts is received at port 2. S-parameters represent loss in the device, so graphs of S-parameters are restricted to negative values of magnitude in dB and positive values of frequency. An example of an S-parameter plot is shown below in Figure 3-2.

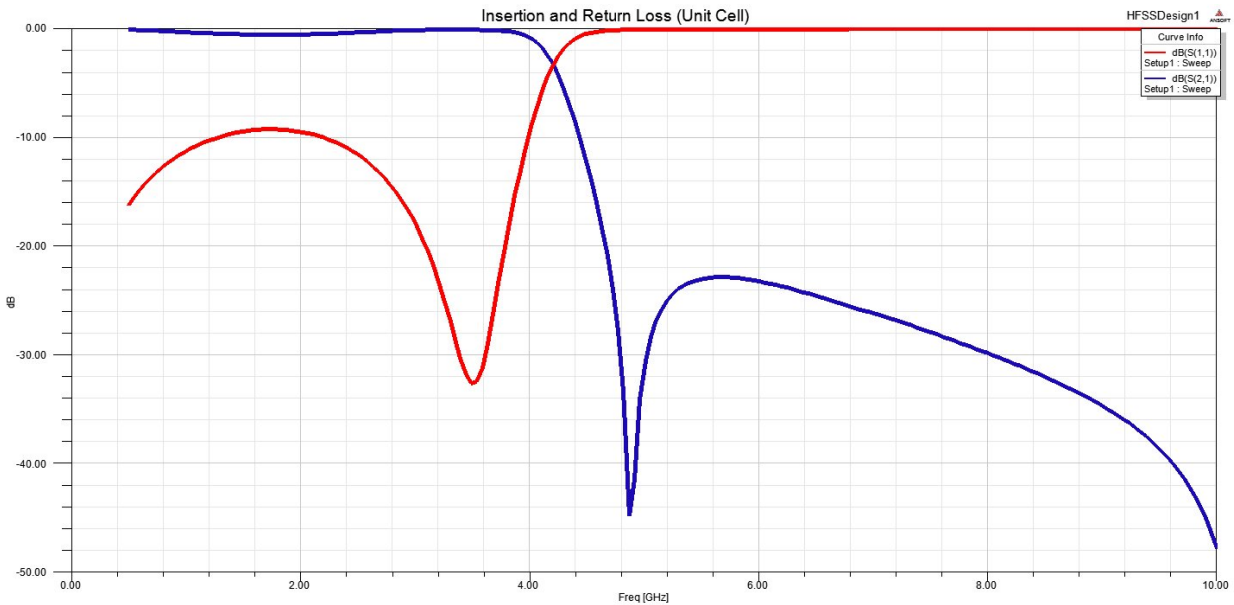


Figure 3-2: S11 (red) and S21 (blue) plot of a low-pass filter.

Shown above is the S11 and S21 plot of a microwave filter, also known as the filter's frequency response. It can be seen that at lower frequencies the value of S11 in red is -10dB or lower while after about 4GHz the magnitude of S11 is close to 0dB. This means that at frequencies below 4GHz the filter reflects relatively small portions of the signal, and at frequencies above 4GHz nearly the entire input signal is reflected. Similarly, the magnitude of S21 at frequencies below 4GHz is close to 0dB while at frequencies higher than 4GHz the magnitude of S21 continues to become more negative. This means that at low frequencies a signal can be transmitted through the filter with little transmission loss, while at higher frequencies the power loss of the signal is significant as it travels through the device. By rejecting these higher frequency signal components and passing the lower frequency components, this device demonstrates low-pass filter behavior.

When describing microwave filters and their frequency responses, there are some commonly-used measures of performance and terms that aid in filter analysis and design. One such parameter is the center frequency, often denoted as f_c . The center frequency of a filter is the central frequency of the device between the upper and lower cutoff frequencies, the frequency boundaries

where the response changes from a passband to a stopband or *vice versa*. The cutoff frequencies often define the frequency region where the device acts in a desired manner, otherwise known as the bandwidth. The bandwidth most common in filter analysis is the -3dB bandwidth, where the cutoff frequencies are defined at the points on the graph where the S-parameter magnitude is -3dB, signifying a point where the power of the signal is one-half the maximum power.

Passive RF and microwave filters are often represented by lumped element models—circuits composed of series and parallel or shunt combinations of capacitor and inductor components. These lumped element models are usually presented as one of two dual types of network configurations, namely the T-section network and the π -section network. An example of a T-section network and a π -section network are shown below in Figure 3-3.

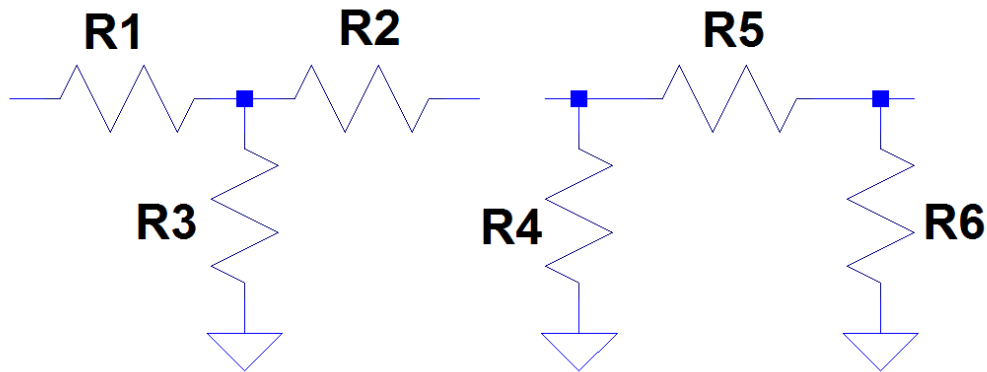


Figure 3-3: T-section and π -section models of a lumped element filter.

The T-section network starts with a series element that is connected on a single end to both a shunt element and another series element, making a “T” shape. Similarly, the π -section model begins with a shunt element connected to a series element that is also connected to another shunt element on the opposite end, making a sort of “ π ” shaped network. Both T-section and π -section models are generally symmetrical and contain an odd number of elements in order to take advantage of this symmetry.

Most simple microwave filters can be classified into four different types, depending on the behavior of their frequency response. First is the aforementioned low-pass filter, where lower frequency components of a signal pass through the device while higher frequency components are attenuated. The lumped element T-section and π -section models of the low-pass filter are shown below in Figure 3-4.

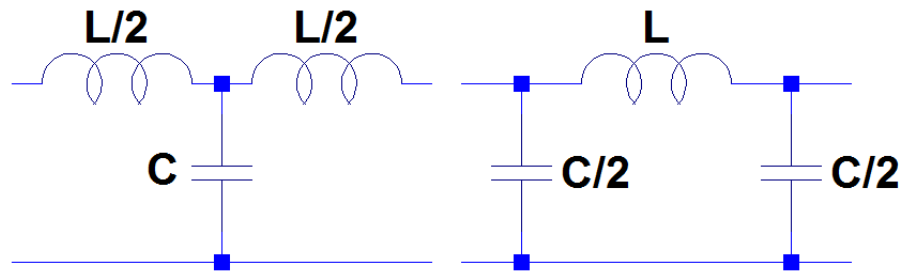


Figure 3-4: Left: T-section model of the low-pass filter. Right: π -section model.

In the low-pass filter models, the inductors serve as the series elements while the capacitances serve as the shunt elements. At DC and frequencies below the cutoff frequency, the capacitance acts like an open circuit, and the current flows through the inductances along the path. At high frequencies (above the cutoff frequency), current flows into the capacitors, effectively short-circuiting the line to ground. This results in a low amount of power being transmitted through the device at higher frequencies.

The opposite of the low-pass filter is the high-pass filter. In the high-pass filter, frequency components above the cutoff frequency are allowed to pass through the device while frequency components below the cutoff frequency are attenuated. The T-section and π -section models of the high-pass filter are shown below in Figure 3-5.

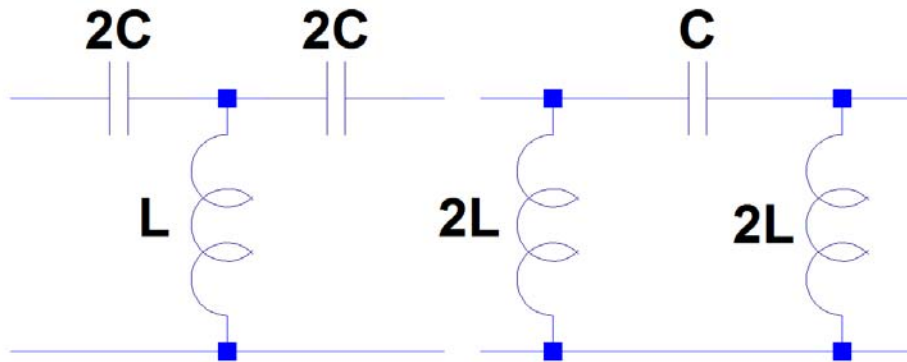


Figure 3-5: Left: T-section model of the high-pass filter. Right: π -section model.

In the high-pass filter model, the capacitance serves as the series element while the inductance serves as the shunt element. At DC and low frequencies, the inductor in the model behaves like a short-circuit to ground, preventing signal propagation. At higher frequencies, the inductor begins to act as an open circuit and the signal propagates. The low-pass and high-pass filters are duals in nature and can be transformed back and forth by replacing capacitances with inductances and inductances with capacitances.

In addition to low-pass and high-pass filters, there exist also the band-stop or notch filter and the band-pass filter. The band-stop filter is unique in that it is designed to allow all frequencies from DC onward except for a certain band of interest. In this band, called the stopband, signal propagation is impeded, while signal propagation is allowed elsewhere. In the band-pass filter, the opposite is true—only a single band of interest is passed, while signal propagation at frequencies both lower and higher than the cutoff frequencies is inhibited. Lumped element models of both the band-stop and band-pass filters are shown below in Figure 3-6 and Figure 3-7.

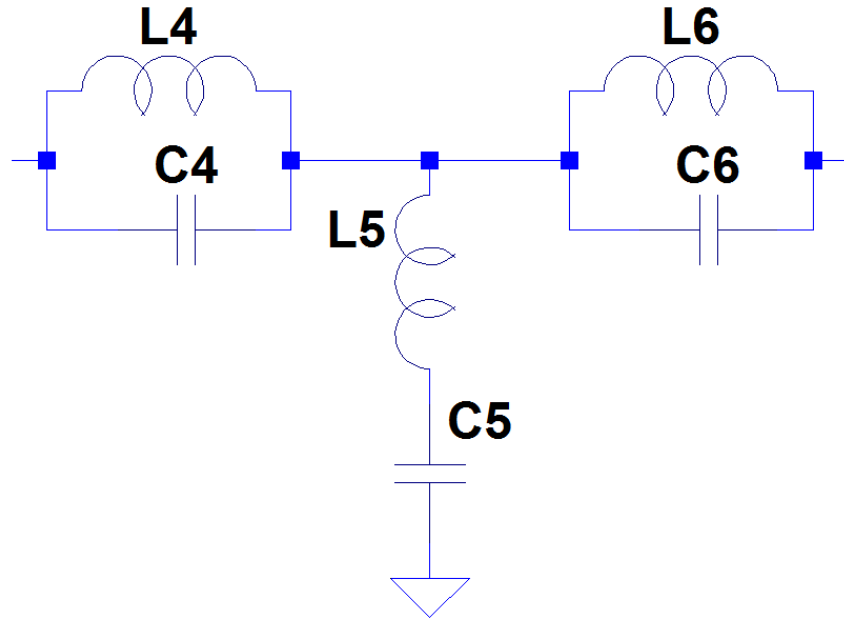


Figure 3-6: Lumped element model of the band-stop filter.

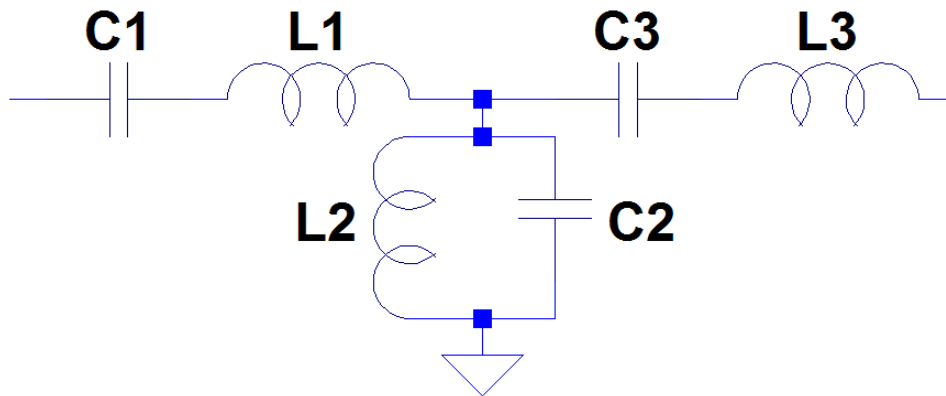


Figure 3-7: Lumped element model of the band-pass filter.

It can be seen by the series arrangement of shunt combinations of capacitance and inductance that the band-stop filter is designed to pass signal components at all frequencies except those around the center frequency, while the series arrangement of series elements in the band-pass filter allows the device to block out most frequency components except those around the center frequency.

Several different technologies have been proposed for the design of electronic filters. Analog passive filters like those shown previously can be fabricated using simple arrangements of sheets of metal that act as capacitive and inductive elements, and these filters, while simple, require no power source to operate. Active analog filters can also be designed by adding powered components like operational amplifiers. In addition to these simpler types of devices, some more novel designs have been presented.

Digital filters have been realized and allow for operation on discrete-time signals as opposed to the real-time signals used by analog filters. [23] Since software and microprocessors can be introduced to the design of these digital filters, much more complex filter designs are possible. Additionally, digital filters are not as vulnerable to component tolerances and errors. A digital filter generally consists of an analog-to-digital converter to convert the analog signal to some digital input, some computer program running on a processing unit to filter the data, and a digital-to-analog converter to convert the digital output back to an analog signal. While digital filters, especially higher order versions, can take up less space in a circuit, they are limited with respect to analog filters by their power consumption, inherent latency, and noise and information loss through the conversion processes.

Several types of mechanical filters have also been proposed. [24] These filters take advantage of transducers at the input and output ports to convert electrical signals into mechanical vibrations and *vice versa*. These filters are analogous to electronic filters in design and analysis but are capable of achieving much higher values of quality factor Q and, subsequently, selectivity. RF microelectromechanical systems (MEMS) filters, a subset of mechanical filters, is a relatively recent technology in the design of mechanical filters and has made possible the construction of high Q filters of small size. [25]

The surface acoustic wave (SAW) filter is an electromechanical device that combines aspects of electronic and mechanical filters into one application. [26] An RF signal on the input side is converted to an mechanical wave that travels across the surface of a substrate made of ceramic, piezoelectric crystal, or a similar material. On the output end, a delayed version of the signal is converted from an acoustic wave back to an RF signal. A similar device to the SAW filter is the bulk acoustic wave (BAW) filter, which uses thin-film technology and standing waves to filter at higher RF frequencies than SAW technology. [27]

To realize filters in microelectronic technology, one common approach is the planar microstrip transmission line design. Microstrip offers several engineering advantages, including ease of integration with active and passive devices, the ability to be micromachined using photolithographic processes, compact size, light weight, and cost. In microstrip design, a flat metal conducting strip (such as copper) is placed on a relatively large but electrically thin dielectric substrate with a ground plane on the bottom. An example of a microstrip transmission line is shown below in Figure 3-8.

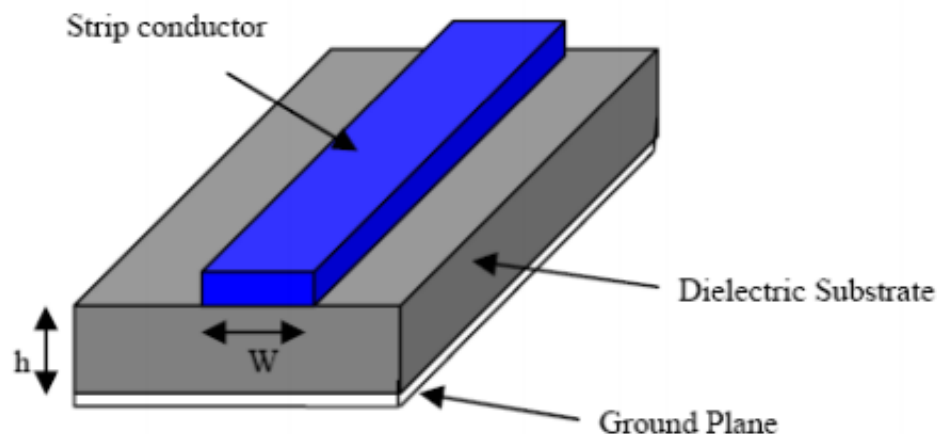


Figure 3-8: A simple microstrip transmission line. [28]

The physical features of a microstrip transmission line play a large role in the performance of the device. Sheets of metal on the substrate that compose the signal line can represent lumped elements or combinations of lumped elements, depending on their shape. This allows for the construction of microwave filters on a substrate without any actual lumped element components. For example, an open-ended microstrip line can be represented as a transmission line terminated in a capacitance. Microstrip filters often have signal lines that vary in width over the length of the line with pieces of line of differing width and length attached to the main line. Two properties of microstrip that are relevant to this work are the fact that series etched gaps in microstrip can be modeled as a capacitance and shunt stubs of line can be represented as impedance. [29]

For the construction of metamaterial filters at RF and higher frequencies, special consideration must be given to the type of dielectric substrates of these devices for various reasons including cost, ease of fabrication, dielectric constant, RF properties, and in this case, flexibility. In this work, all filter designs are presented using the microstrip transmission line filter approach using a liquid crystal polymer (LCP) substrate. LCP is more commonly used in MEMS design than in metamaterials, although there has been recent work using LCP as a metamaterial substrate. [30][31] LCP is chemically unreactive, has a low dielectric constant of 3.1, is mechanically strong, is thermally stable, and is readily commercially available. A common use for solid LCP is in Kevlar products, and when purchased from a manufacturer LCP is generally laminated on one or both sides with copper cladding. LCP can reportedly be useful as a substrate for frequency applications beyond 40GHz because it is not as lossy as conventional RF materials at higher frequencies. [32] [33] In [33], it is claimed that LCP offers a low loss tangent at frequencies as high as 110GHz.

LCP can exist in both a liquid phase and a solid phase, but in its solid phase it can be treated as a rigid structure for the purposes of micromachining and microelectronic fabrication while still

being flexible enough to conform to curved and other nonplanar surfaces. When fabricated as a thin film, LCP can be as conformal to surfaces similar to a sheet of paper at thicknesses as small as 1 mil without becoming brittle. Some examples are shown below in Figure 3-9.

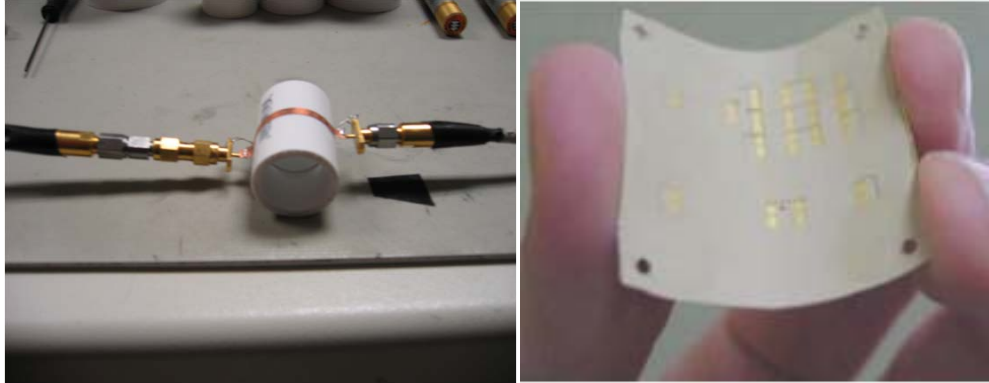


Figure 3-9: Left: LCP substrate curved over PVC pipe. [30] Right: Demonstration of the flexibility of LCP. [33]

Chapter 4

Metamaterial Filters

As mentioned in the previous chapter, transmission lines laden with resonating metamaterial elements experience backward wave propagation due to negative index of refraction over a certain frequency range defined by the structure of the device. In this sense, a metamaterial device can be considered a frequency-selective structure (FSS), a periodic structure that responds to electromagnetic fields based on frequency. At certain frequencies, current induced in an FSS will transmit power from an incident wave through the structure; however, at other frequencies the FSS will inhibit or reflect an incident wave. Because of this behavior, FSSs are often considered a type of filter.

Due to their resonant nature, compact size, straightforward implementation, and ease of fabrication, metamaterial structures have become a common choice for novel RF and microwave planar filter designs. Indeed, simply loading a transmission line with SRRs or CSRRs will inhibit wave propagation near the resonant frequency due to the negative-index nature of the resonant elements. In the SRR case, the addition of shunt stubs will generate backward wave propagation, and the same effect can be accomplished in the CSRR case using etched series gaps instead. In addition to this, it is possible to combine shunt stubs and series gaps in a metamaterial transmission line to achieve well-known types of filters—different configurations of these stubs and gaps can be used to realize low-pass filters (LPF), high-pass filters (HPF), band-stop filters (BSF), and band-pass filters (BPF). Over time, patterns have emerged in the design of these types of filters, making it easy to determine the type of a metamaterial filter by observing the presence or lack of shunt stubs and series gaps in the signal line. In this work, the design of CSRR-loaded RF and microwave metamaterial filters using microstrip technology will be examined exclusively.

A CSRR-loaded microstrip LPF is generally characterized by the presence of narrow shunt stubs attached to the main signal line directly above the CSRR ring section, usually on the sections of line between ring elements. An example of a metamaterial LPF using square CSRRs and its frequency response is given below in Figure 4-1.

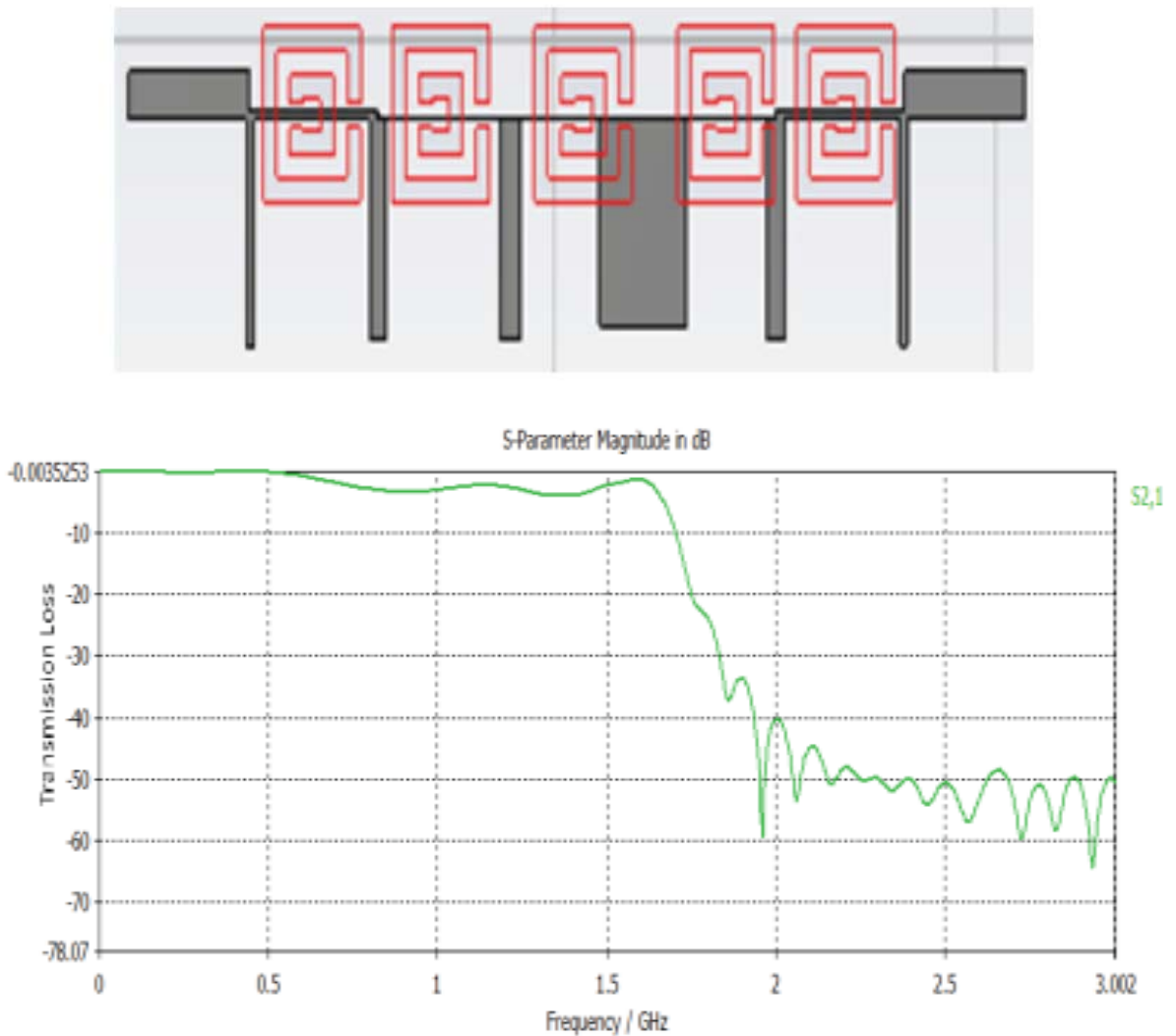


Figure 4-1: Above: Example of a CSRR-loaded low-pass filter using shunt stubs.

Below: Frequency response of the CSRR-loaded low-pass filter. [34]

As shown above, shunt stub elements of varying width and length are located above the region that includes the metamaterial rings. Also, it is notable that there are no series gaps etched into the

signal line in the LPF, although the signal line does visibly narrow and widen over the CSRR region.

To better understand the form of the CSRR LPF, the CSRR-loaded transmission line in Figure 2-9 can be compared to the lumped element model for a simple LPF. The lumped element model of the LPF from Chapter 3 is shown below in Figure 4-2.

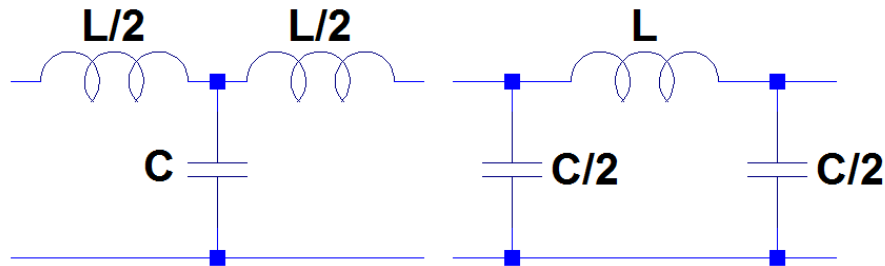


Figure 4-2: Left: T-section form of a lumped element LPF. Right: The π -section form.

In both the T-section and π -section models, the filter is composed of a series inductance connected to a shunt capacitance, which allows the filter to pass low-frequency signals while blocking signals at higher frequencies. By adding inductance to the signal line of the CSRR filter, the low-pass characteristic can be made to dominate the frequency response of the device, resulting in a LPF.

The CSRR-loaded HPF can be explained in a similar manner to the LPF. CSRR-loaded microstrip HPFs are characterized by their series gaps in the signal line above the CSRR rings and the lack of large shunt stubs on the line between CSRR elements. Some examples of CSRR metamaterial HPF designs are shown below in Figure 4-3 along with the frequency response of each design.

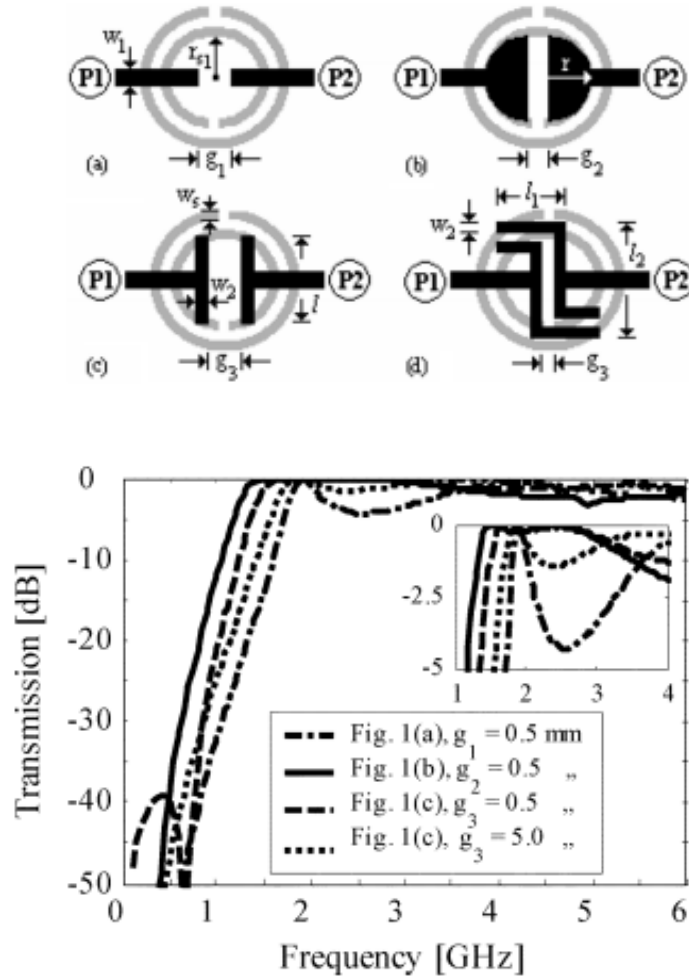


Figure 4-3: Above: Different signal line designs for a CSRR-loaded HPF. Below: Frequency response of the four HPF designs. The HPF design is characterized by the series gap in the signal line above the CSRR rings. [35]

In each of the four designs above, a gap in the signal line is etched directly above the center of the CSRR element in the ground plane. This is particularly notable because the shunt stubs in the LPF sit between elements while the series gaps in the HPF are directly above the elements—a type of duality in the physical design of the signal lines. The series gaps shown above are capacitive in nature, which leads to the addition of a series capacitance in the lumped element model of the filter. While small shunt stubs or other additions to the line around the series gap are possible, these additional pieces of line are short and usually are restricted to the area directly above the CSRR rings to prevent the inductance of the line from dominating the gap capacitance.

For the HPF case, the lumped element model of the HPF from Chapter 3 is shown below in Figure 4-4.

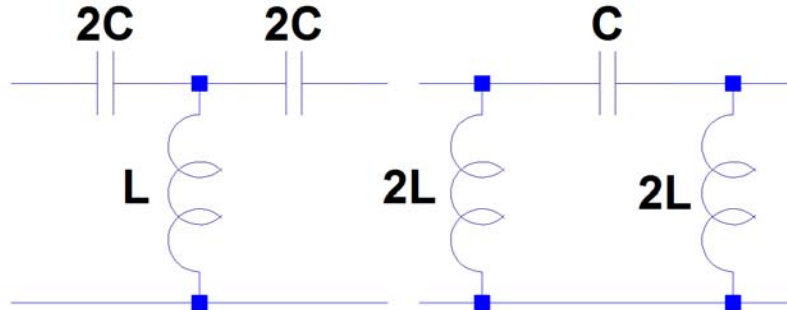


Figure 4-4: Left: T-section from of a lumped element HPF. Right: π -section form.

Comparing the models in Figure 4-4 to that in Figure 2-9, it can be seen that the capacitive gap C_g serves as the series capacitance in the CSRR high-pass model. In the design, this capacitance allows the high-pass component of the filter to dominate the frequency response in the negative-index region, resulting in a CSRR-loaded HPF.

While the LPF and HPF require adding material to or removing material from the host line, designing the metamaterial band-stop filter using CSRRs is relatively simple. While the low-pass and high-pass filter designs seem to require additions or subtractions to the host line, it has been shown that a band-stop filter can be realized by simply etching CSRR rings underneath a microstrip transmission line and substrate [36]. Using no series etched gaps or shunt stubs, a narrowband stop-band filter was designed where the three CSRR elements were located at symmetric periodic points in the ground plane. A picture of the band-stop filter design is shown below in Figure 4-5.

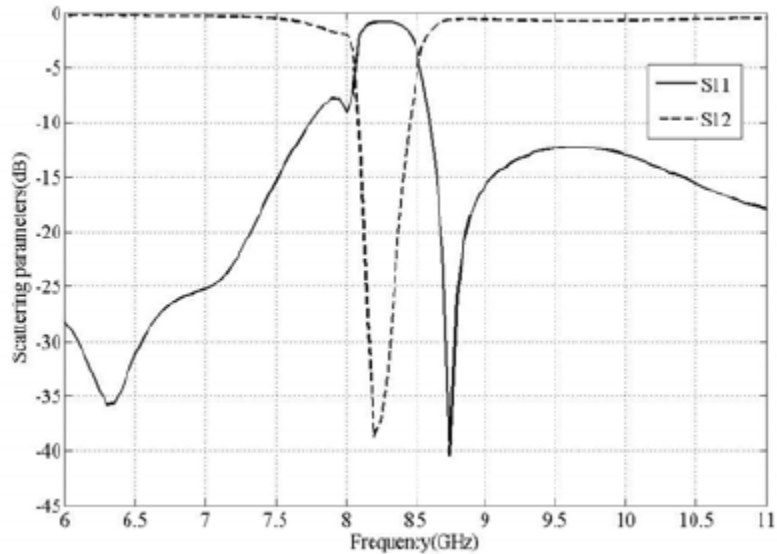
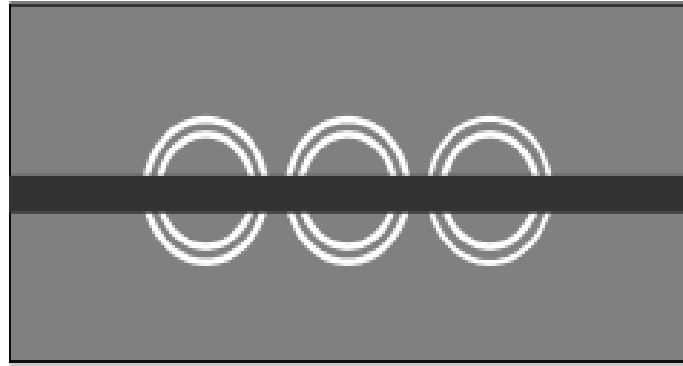


Figure 4-5: Above: CSRR band-stop filter design. Below: Frequency response of the band-stop filter.

The band-stop filter requires no series gaps or shunt stubs in the host line. [36]

While this result may seem unintuitive, it is important to remember that SRR- and CSRR-loaded transmission lines reject signal propagation naturally—an impedance-matched signal line represents a balance between low-pass and high-pass structures, therefore blocking signals at frequencies above and below resonance.

Finally, it is also possible to design band-pass filters using CSRR metamaterial technology. By examining the types of signal line features presented in the previous three types of filters and understanding their purpose, a concept for the design of a CSRR-loaded band-pass filter can be

easily conceived. A band-pass filter can loosely be considered as a combination of low-pass and high-pass filters with an overlap resulting in a small frequency band where signal propagation is permitted. By this reasoning, an attempt at a CSRR-loaded band-pass filter could be made by combining signal line designs from both LPFs and HPFs on a single host line. Much like the BSF, metamaterial BPFs take advantage of a balance between these low-pass and high-pass elements. An example of this concept is given below in Figure 4-6.

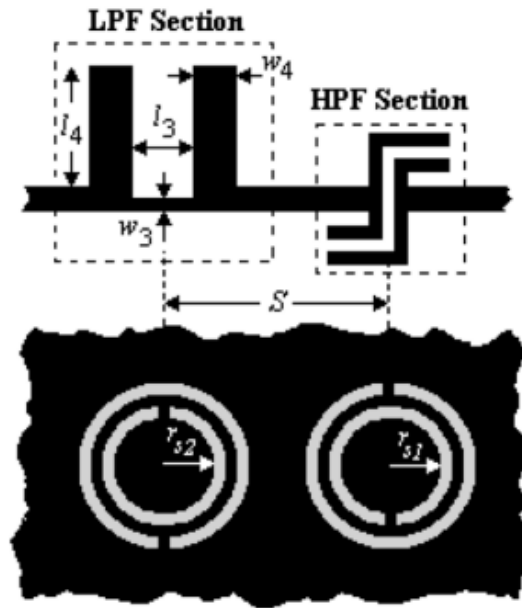


Figure 4-6: CSRR band-pass filter design. Left: The low-pass component with shunt stubs. Right: The high-pass component with series gap. [35]

Figure 4-6 shows that a band-pass filter can be realized using cascading low-pass and high-pass signal elements above CSRR structures on a single host line. In this way, the two cutoff frequencies of the low-pass and high-pass sections serve as the upper and lower cutoff frequencies of the BPF and result in a passband that can be increased or decreased by adjusting the dimensions of the structures. The lumped element model of the CSRR BPF can be examined as before and is shown below in Figure 4-7.

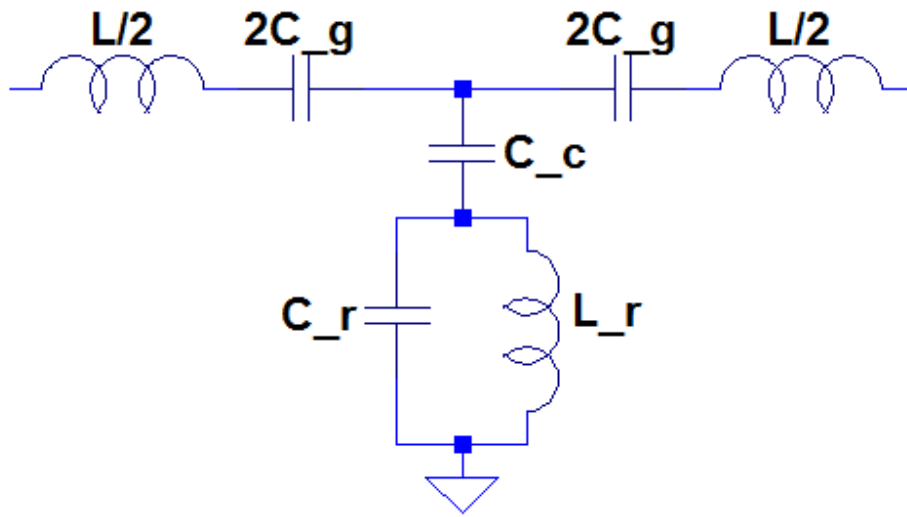


Figure 4-7: Lumped element model of the CSRR-loaded BPF.

In the lumped element model above, L represents the inductance of the host line, C_g represents the capacitance of the etched gap, C_c models the electric coupling capacitance, L_r represents the ring inductance, and C_r models the ring capacitance. As explained earlier, when adding etched capacitance to a CSRR-loaded transmission line, the capacitance will dominate the frequency response at the resonant frequency, resulting in a HPF. In this instance, the CSRR-loaded HPF can be converted to a BPF by increasing the inductance of the filter at resonance. This can be achieved by adding shunt stubs of line from the LPF design concept to increase the line inductance.

Since the behavior of the CSRR-loaded BPF can be easily adjusted, this filter in particular leaves the designer with the ability to finely tune the frequency response of the device. In [36], a metamaterial BPF was designed with cutoff as sharp as 50 dB at the lower and upper cutoff frequencies. The frequency response is shown below in Figure 4-8.

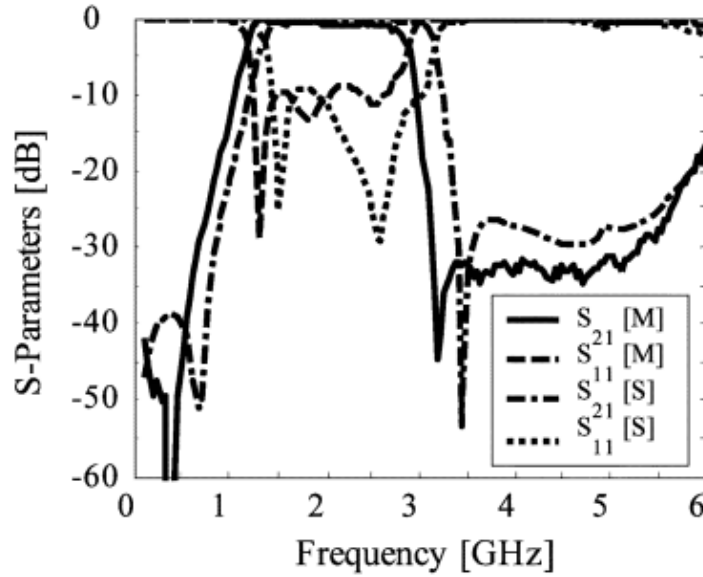


Figure 4-8: Frequency response of a CSRR-loaded band-pass filter. [35]

While the cascading low-pass and high-pass design results in a suitable BPF, the very nature of the metamaterial BPF lends itself to several different but viable combinations of signal line elements. Theoretically, any combination of capacitive etched gaps and inductive shunt stubs of line would result in some type of band-pass behavior. In [31], a BPF was demonstrated using only a capacitive gap and no shunt stubs; the filter and its frequency response is shown below in Figure 4-9 and 4-10.

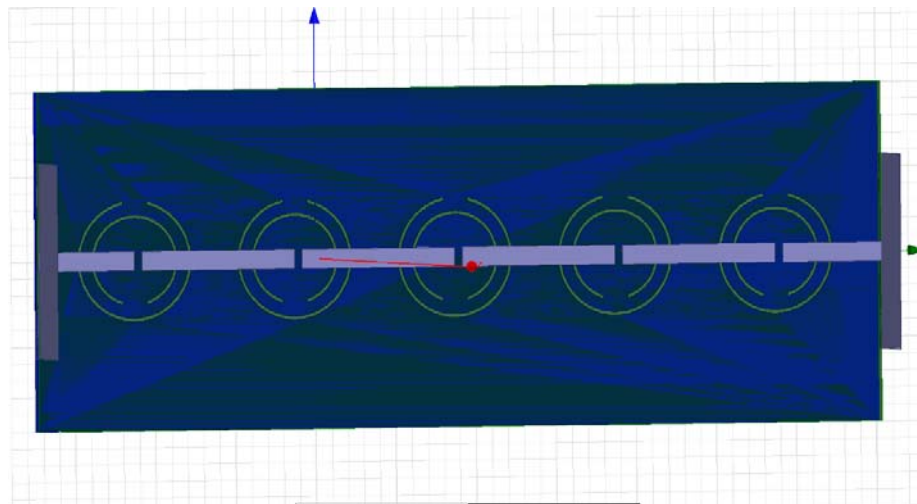


Figure 4-9: Planar CSRR-loaded BPF using only etched capacitive gaps. [31]

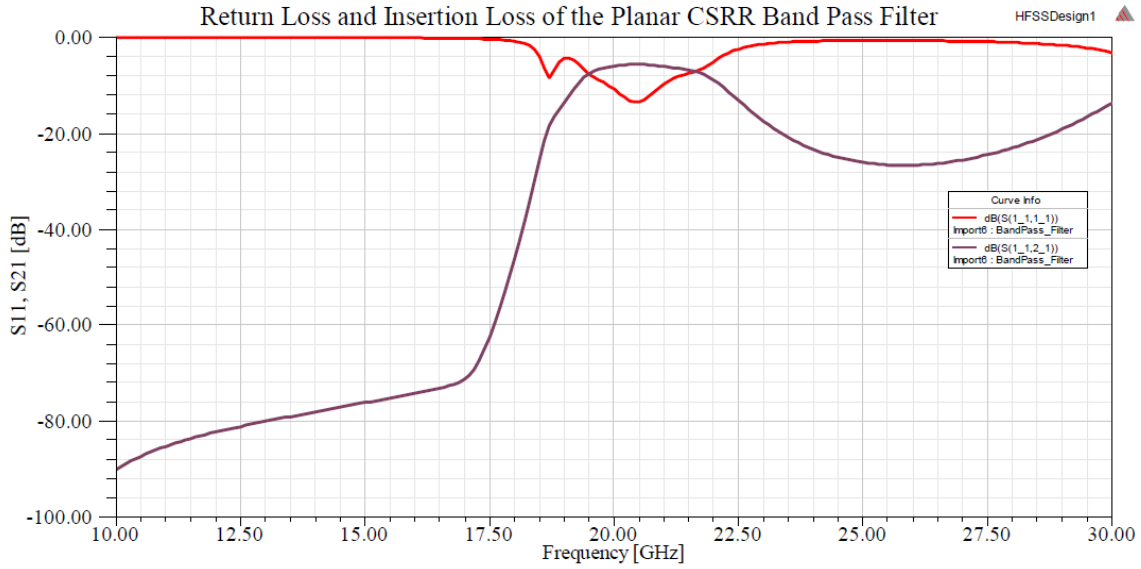


Figure 4-10: Frequency response of the BPF shown in Figure 4-9. [31]

In [37], a BPF was designed that used only a single signal line element combining series gaps and shunt stubs above a CSRR. This design incorporated additional capacitive gaps and inductive lines on the signal line in an attempt to sharpen the upper band performance of the frequency response and inspired the design presented in this work. The filter and its frequency response are shown in Figure 4-11 and Figure 4-12.

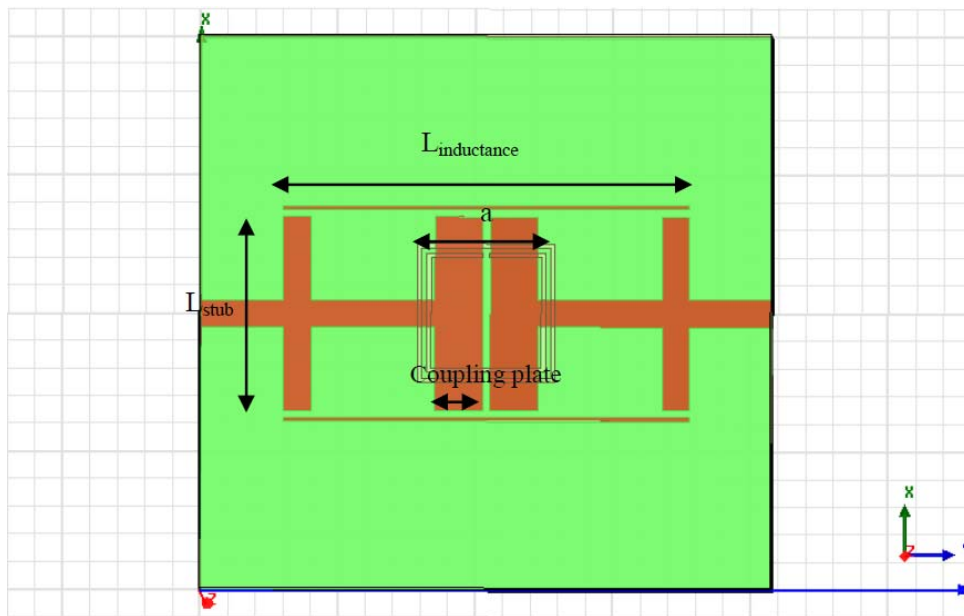


Figure 4-11: CSRR-loaded BPF with a single element above the metamaterial structure. [37]

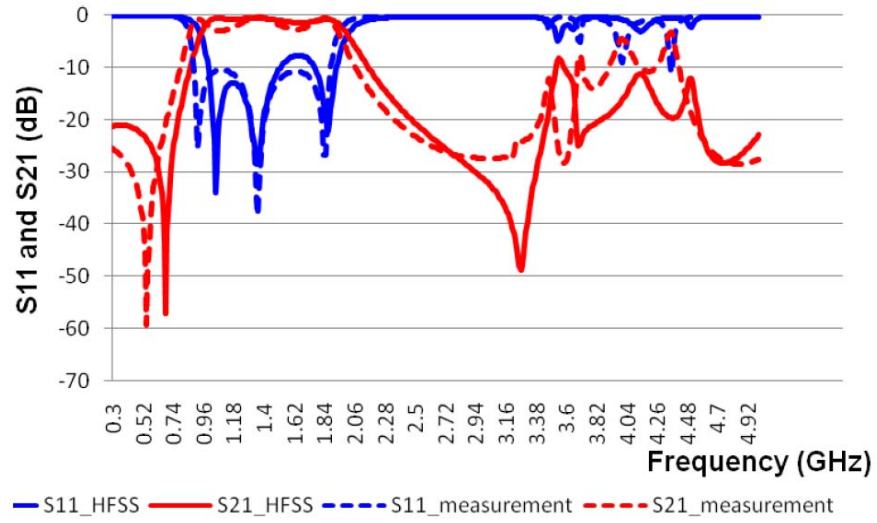


Figure 4-12: Simulated and measured frequency response of the BPF shown in Figure 4-11. [37]

Chapter 5

HFSS

In this work, Ansys HFSS was used to design and simulate all metamaterial filter models. This commercial electromagnetic modeling and simulation software uses the Finite Element Method (FEM) to solve three-dimensional microwave structures such as antennas, transmission lines, oscillators, and in this case filters. In HFSS, the user is able to draw a structure using predefined shapes such as boxes, spheres, and cylinders, create custom shapes using several editing options, and simulate an extensive list of electromagnetic parameters such as S-parameters over variables such as frequency or physical dimensions. HFSS is also able to show and animate electromagnetic fields traveling through and across a device in both magnitude and vector forms. To simulate a structure, the user must define the boundaries and excitations of the model after selecting a solution type. HFSS then uses an iterative solving approach that includes creating meshes and updating the solution by solving adaptive passes over the full frequency spectrum of interest. A short overview of the design and simulation of a simple metamaterial filter will be given in this chapter.

To begin the design of the filter model, the ground plane will be added first. This is done by selecting a "box" shape from the 3D Modeler Draw Solid toolbar. This box must then be added to the model by drawing the box shape in the main design window. First the user must click a point in the drawing window to place one corner, then expand to a two-dimensional plane, then add the third dimension; each step automatically occurs after the previous one when the user clicks the desired location. After placing the box, the shape will appear under "Solids" in the explorer window to the left of the design space. Double left-clicking the default name "CreateBox" will allow the user to change the position of the object and its size in all three dimensions. For this

design, the position of the ground plane will be (0,0,0) and the following dimensions will be defined: XSize="9.28mm", YSize="8.4mm", and ZSize="60.3um". The resulting object should look like Figure 5-1 below.

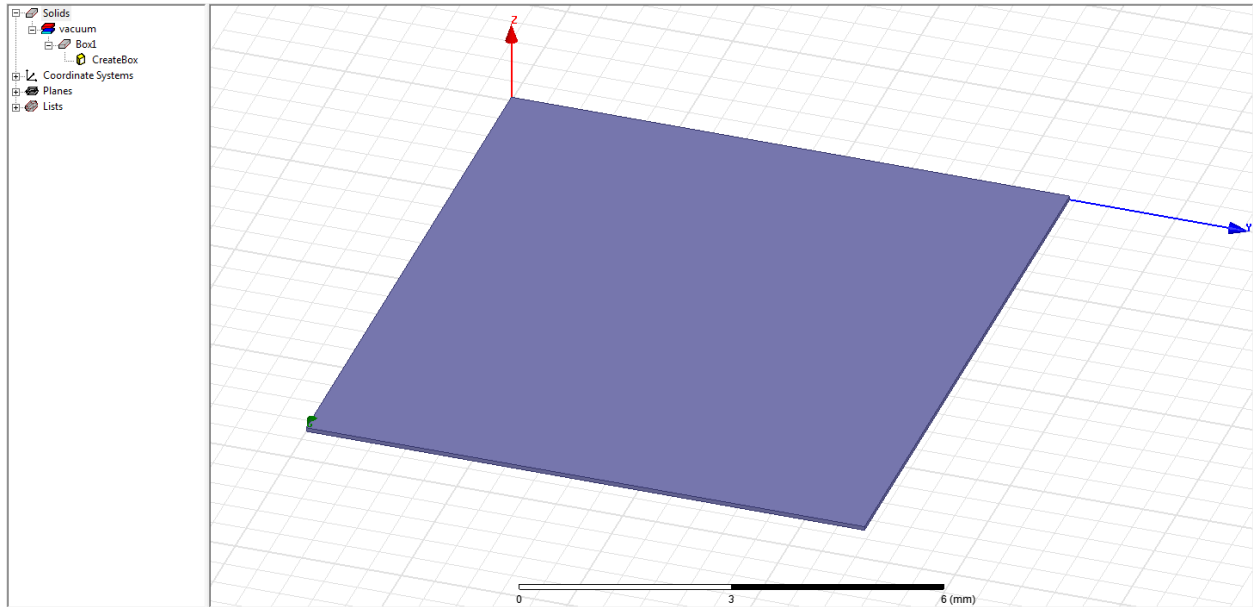


Figure 5-1: Example ground plane layer.

In the explorer window one layer up from CreateBox is Box1, and one level higher is the material definition, which is set to "vacuum" by default. Right-clicking this selection will allow the user to change the name of the object and also the assigned material, among other editing options. In this example the material will be changed to copper by right-clicking Box1, selecting "Assign Material..." from the menu, and selecting Copper from the material definition selection window. The material label in the explorer window on the left will change from "vacuum" to "copper".

Next, the substrate layer will be added. Another box is added to the design window as before with the following dimensions: XSize="9.28mm", YSize="8.4mm", and ZSize="4mil". Additionally, the position of the object should be (0,0,60.3um) to ensure that the substrate layer sits atop the ground plane instead of in the same space. The addition of the substrate layer is shown below in Figure 5-2.

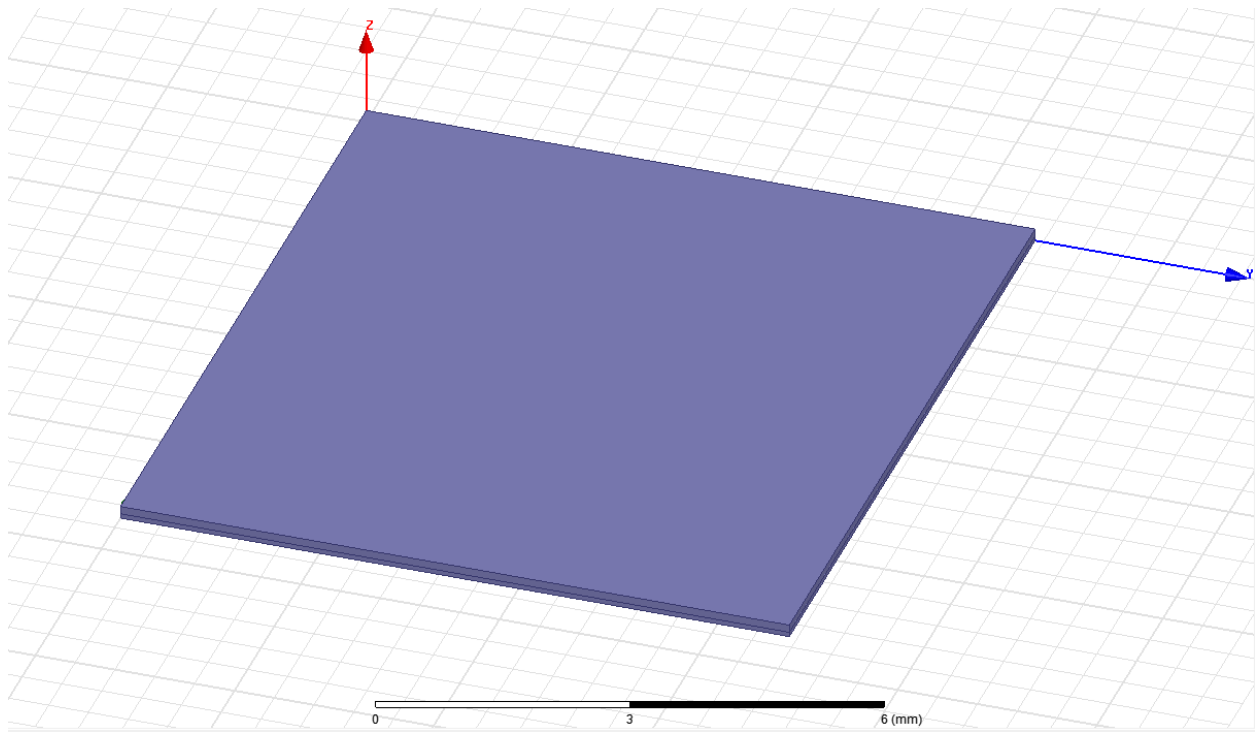


Figure 5-2: Example filter design with added LCP substrate layer.

To define the substrate as LCP, a custom material definition must be added. In the material definition window, select the "Add Material..." button at the bottom. In the View/Edit Material window, set Relative Permittivity to 3.1, Relative Permeability to 1, and Dielectric Loss Tangent to 0.004 for LCP. Name the material LCP and hit OK. Now the substrate layer can be defined as LCP.

Next, the signal line must be added to the model. In this design, a transmission line calculator was used to set the signal line dimensions to match the rest of the microstrip device. For the signal line, define the material as "copper", set the position to (4.176mm,0,0.1619mm) to place the signal layer on top of the substrate and in the middle of the device, and set the following dimensions: XSize="928um", YSize="8.4mm", and ZSize="60.3um". The object should look like Figure 5-3 below.

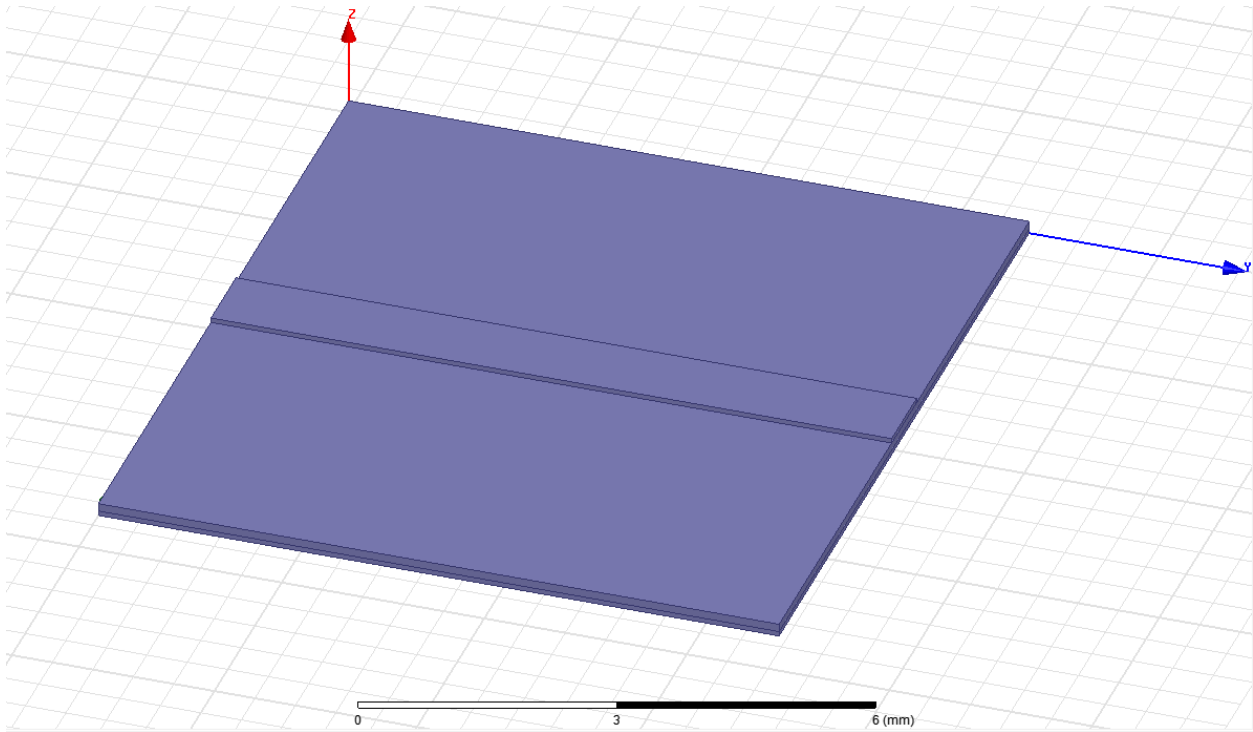


Figure 5-3: Example filter design with copper signal line added.

Next, the metamaterial CSRR rings will be added to the design. To create the rings, two cylinders must be created and then subtracted from the ground plane. Select the Draw Cylinder button next to the Draw Box button and place the cylinder on the device. Right click the cylinder in the explorer window and add the following information: Center Position (4.64mm,4.2mm,0), Radius="3.432mm", and Height="60.3um". This will place the cylinder at the center of the device and will define it as the same height as the ground plane. Define the material of the cylinder as "copper", then add another cylinder using the same process. Right click the second cylinder in the explorer window and define the shape as follows: Center Position (4.64mm,4.2mm,0), Radius="2.7615mm", and Height="60.3um". The two cylinders in the model should look like Figure 5-4 below.

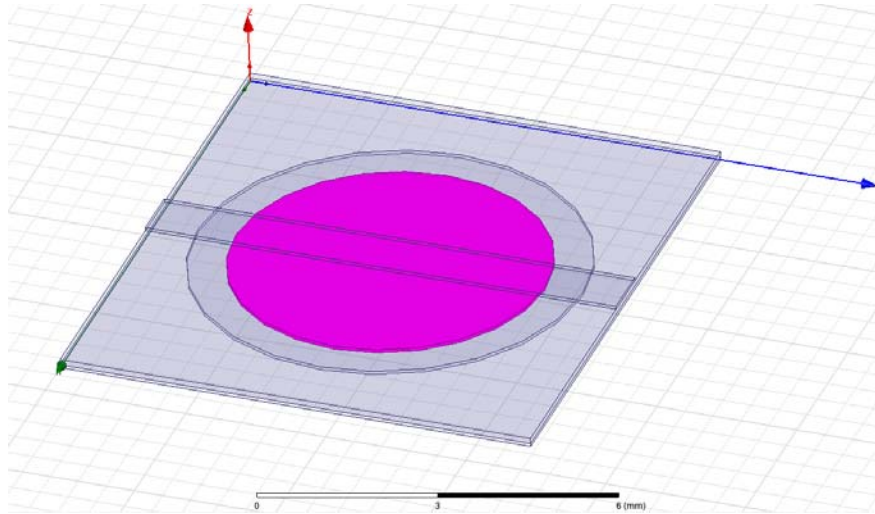


Figure 5-4: Example filter design with both cylinders added for the outer ring.

Next, the smaller cylinder must be subtracted from the larger cylinder to create a ring. To do this, select Cylinder1 and Cylinder2 while holding the CTRL button on the keyboard. Right click Cylinder2, and in the menu go to "Edit">"Boolean">"Subtract...". In the Subtract window, ensure that Cylinder1 is on the left side under "Blank Parts" while Cylinder2 is on the right side under "Tool Parts". Click OK and the smaller cylinder should be removed from the larger cylinder shape, leaving a ring in the ground plane of the device. This ring is shown below in Figure 5-5.

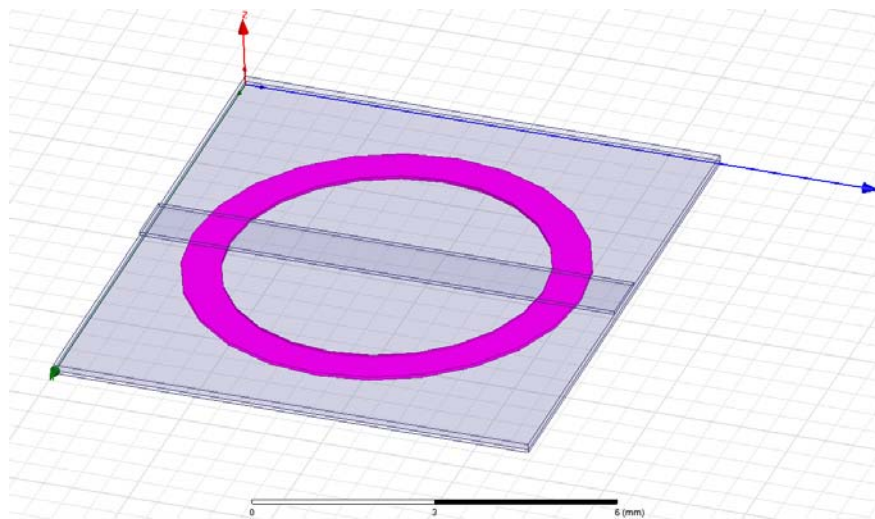


Figure 5-5: Example filter design with the outside CSRR ring shape.

To create the inner CSRR ring, a similar process is used. Create the outer cylinder of the inner ring with the following properties: Center Position (4.64mm,4.2mm,0), Radius="1.2275mm", and Height="60.3um". Create a second cylinder with Center Position (4.64mm,4.2mm,0), Radius="0.9615mm", and Height="60.3um". Subtract the inner cylinder from the outer cylinder as before, and the device should now look like Figure 5-6 below.

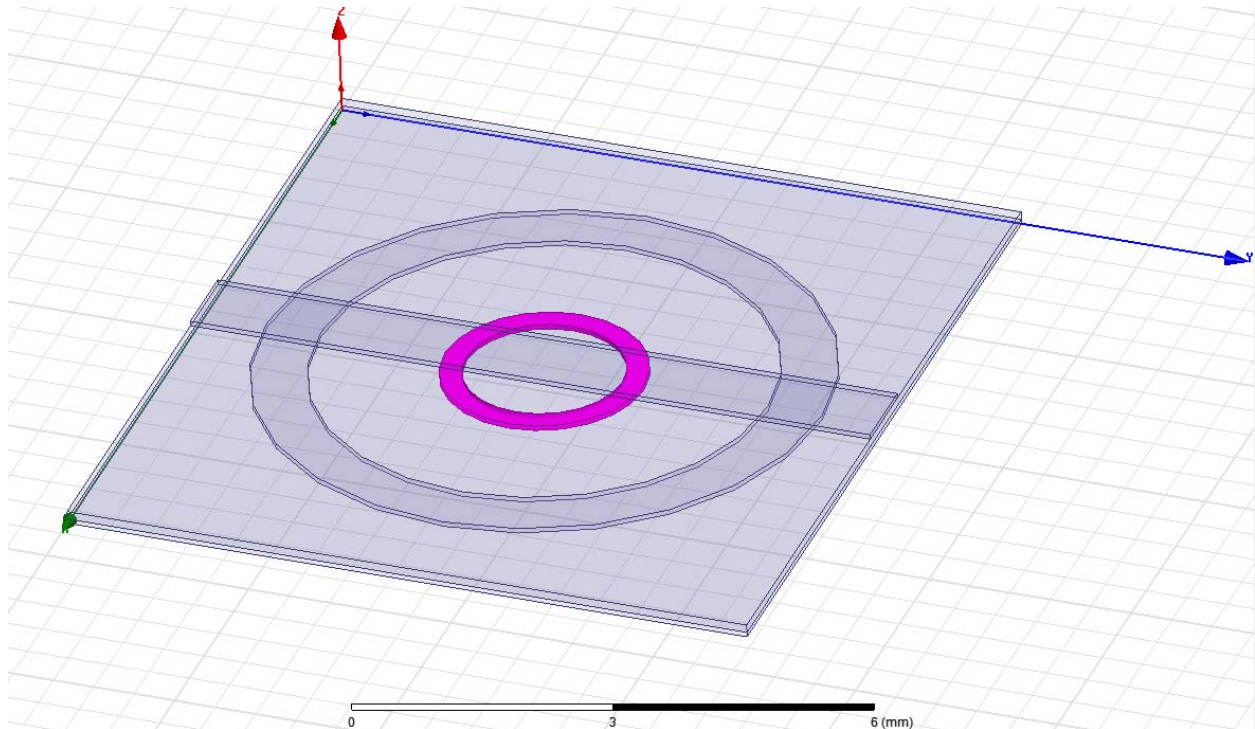


Figure 5-6: Example filter design with both outer and inner CSRR ring shapes.

Next, the ring gaps must be removed from the ring shapes. This will be accomplished by adding two box shapes to the device, one on each ring on opposing sides. Click the Draw Box button and add two boxes to the device. For the outer ring gap, use the following properties: Position (1.208mm,3.35625mm,0mm), XSize="1000um", YSize="1687.5um", and Zsize="60.3um". For the inner ring gap, use the following properties: Position (5.869mm, 3.35625mm,0mm), XSize="-1000um", YSize="1687.5um", and ZSize="60.3um". Use

Edit>Boolean>Subtract to remove the boxes from the two rings, and the device should now look like Figure 5-7 below.

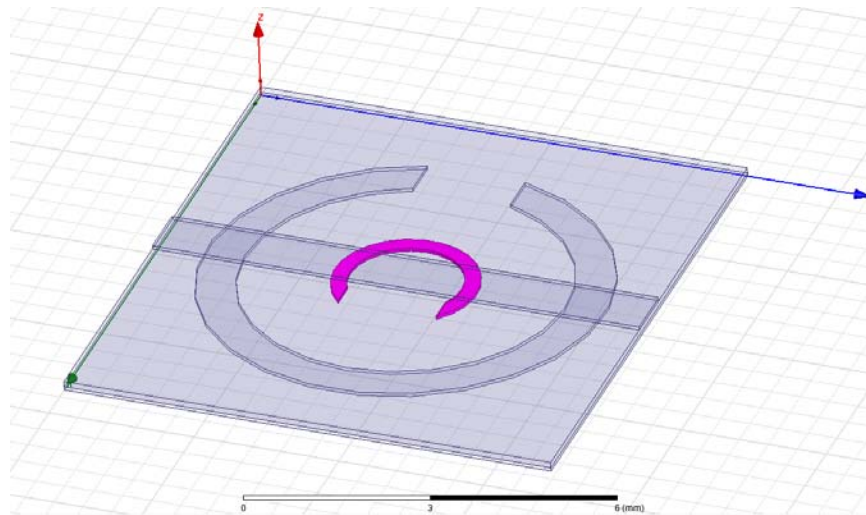


Figure 5-7: Example filter design with ring gaps added.

Finally, the two metamaterial rings must be subtracted from the ground plane to simulate the etching that is done in the fabrication process. Simply select the two rings and go to Edit>Boolean> Subtract and remove the two rings from the ground plane. The end result should look like Figure 5-8 below (the substrate layer has been made transparent so that the rings can be easily seen).

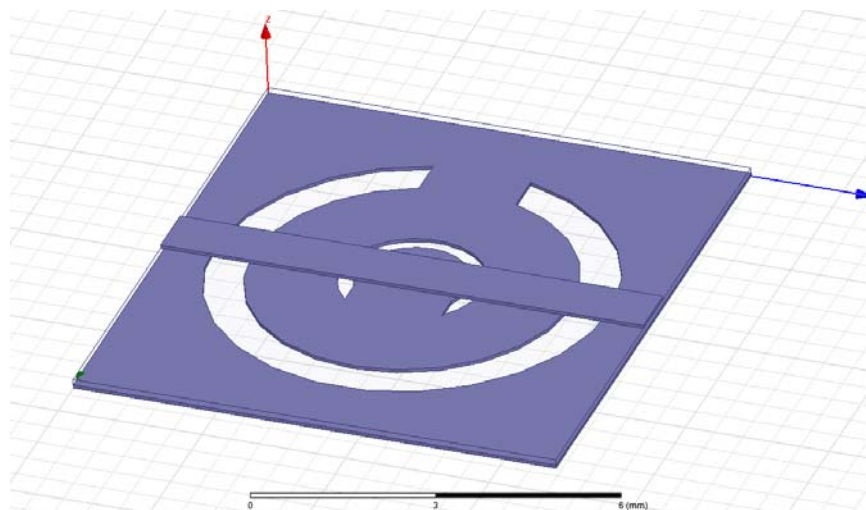


Figure 5-8: Example filter design with CSRR rings removed from the ground plane.

Next, any additions to the signal line must be made. For this design, two shunt stubs will be added to the signal line to create a simple metamaterial low-pass filter. To make these shunt stubs, add two boxes to the design using Draw Box. For the first stub, use the following parameters: Position (1045um,0.675mm,0.1619mm), XSize="7190um", YSize="315um", and ZSize="60.3um". For the second stub, use Position (1045um,7.725mm,0.1619mm), XSize="7190um", YSize="-315um", and ZSize="60.3um". Finally, reassign the material property of the two stubs from vacuum to copper as before. Adding the two stubs to the design should look like Figure 5-9 below.

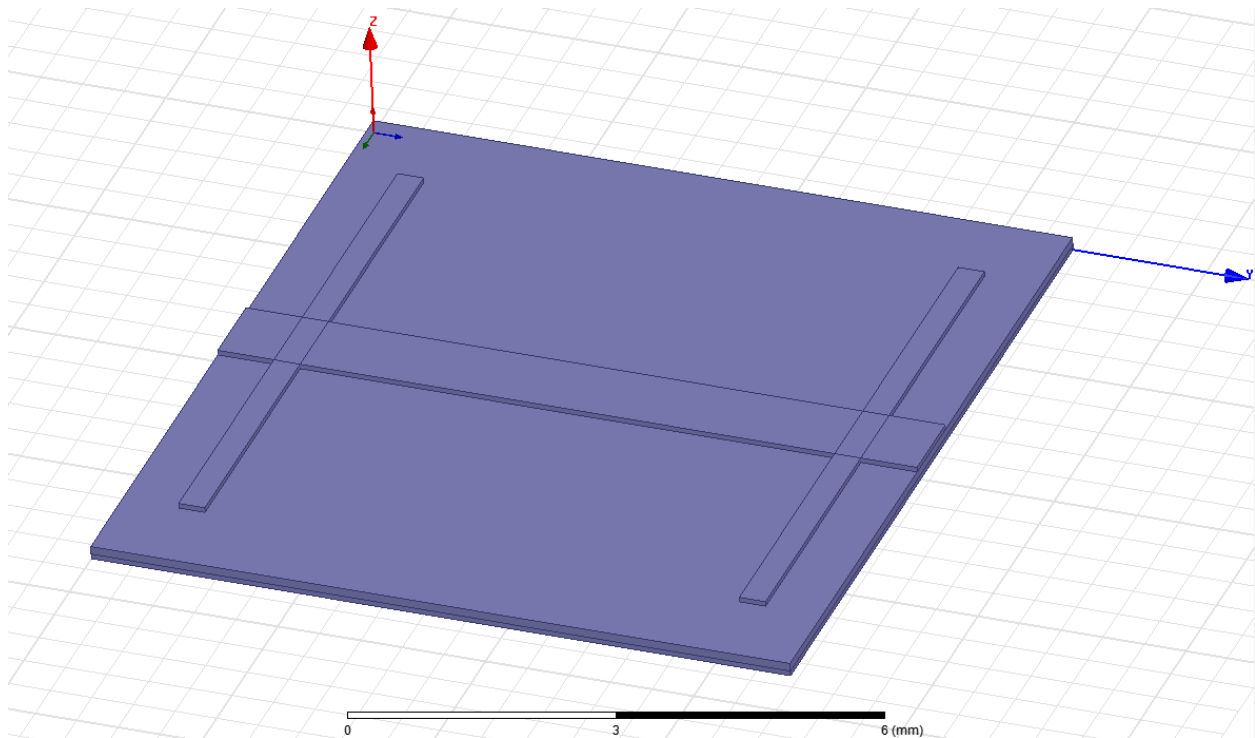


Figure 5-9: Example filter design with shunt stub shapes added.

To add these stubs to the signal line, select the two stubs and the signal line and go to "Edit">"Boolean">"Unite" and add the two stubs to the line, similar to the subtract method from earlier. This will unite the stubs to the signal line, making one signal line object. The final device should look like Figure 5-10 below.

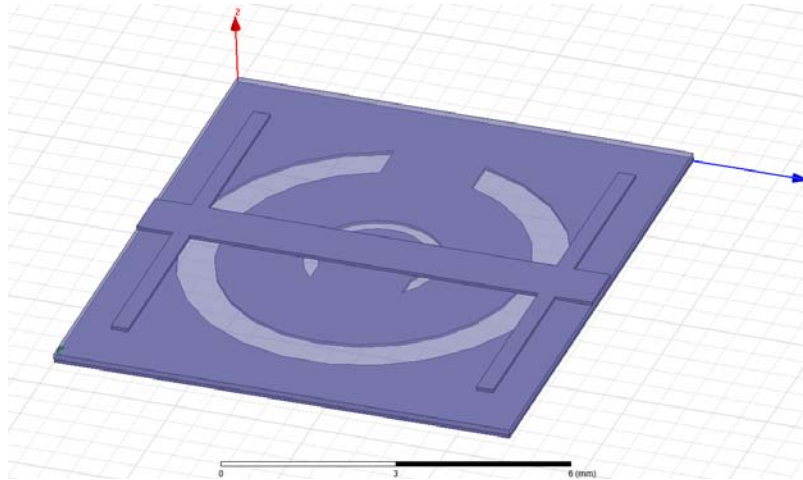


Figure 5-10: Final model of the example filter design.

To simulate the filter, a few external objects must be added to the design. First, a region must be created around the filter to define the simulation region. Click the red and white Create Region button at the right end of the 3D Modeler Draw Objects toolbar. In the new Region window, select the "Pad individual directions" option and set +Z and -Z to "Absolute Position". For +Z set the value to 5mm, and for -Z set the value to -5mm. This will create a vacuum box region that will surround the filter and allow 5mm of space above and below the device. An example is shown below in Figure 5-11.

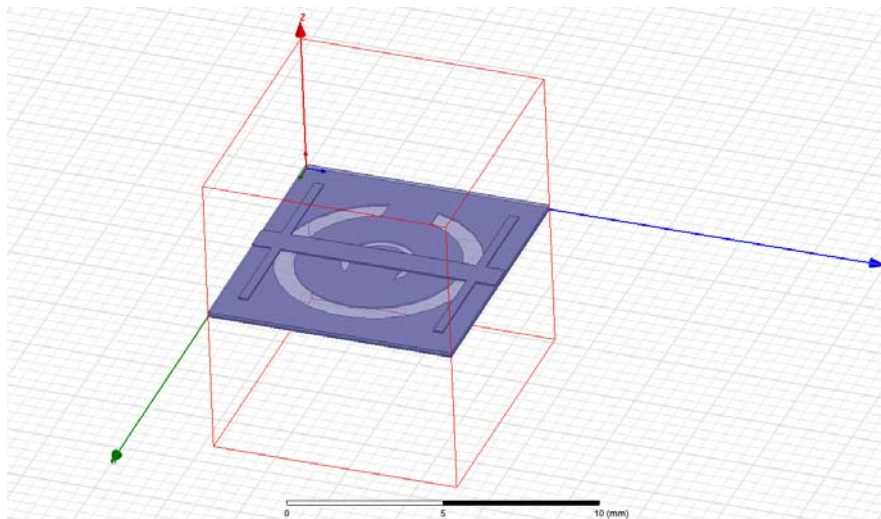


Figure 5-11: Example filter design with boundary region added.

To finishing defining the simulation region, right click the region box and select "Assign Boundary">"Radiation" and click OK.

Next, the two port planes must be added to the terminating sides of the signal line. Click the yellow Draw Rectangle button from the 3D Modeler Draw Sheet toolbar and draw two rectangles, one on each signal line end of the filter. Note that the active plane to draw 2D structures is set to XY, so this may need to be changed to ZX to draw the plane correctly. This can be done by selecting ZX from the drop down menu beside the Draw Region button used previously. The first rectangle should be at position (0,0,0) with an XSize of 9280um and ZSize of 32mil, and the second rectangle should be at position (0,8.4mm,0) with the same XSize and ZSize as the first rectangle. After adding the two ports, the filter design should look like Figure 5-12 below.

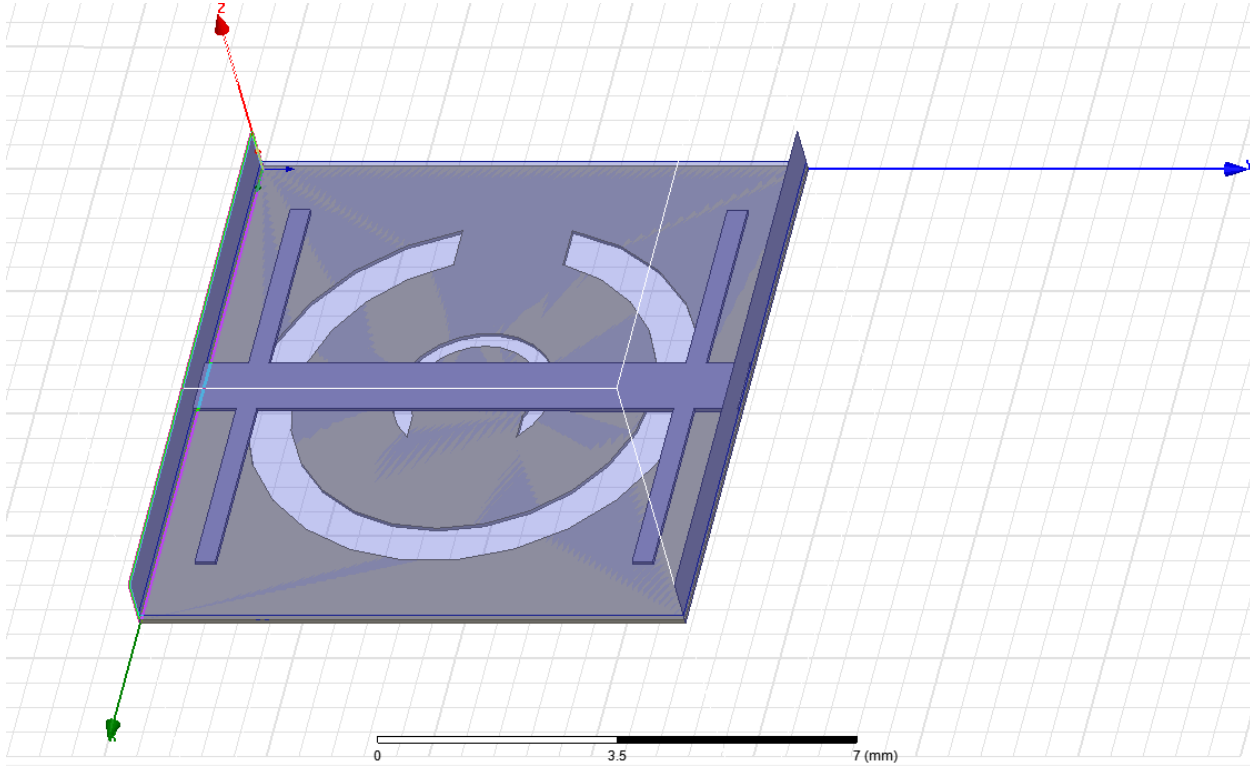


Figure 5-12: Example filter design with port shapes added.

To assign an excitation to these sheets and turn them into ports, right click each rectangle and select "Assign Excitation">"Wave Port". A window asking for the name of the port will appear. After naming the port and clicking next, then the following window will appear:

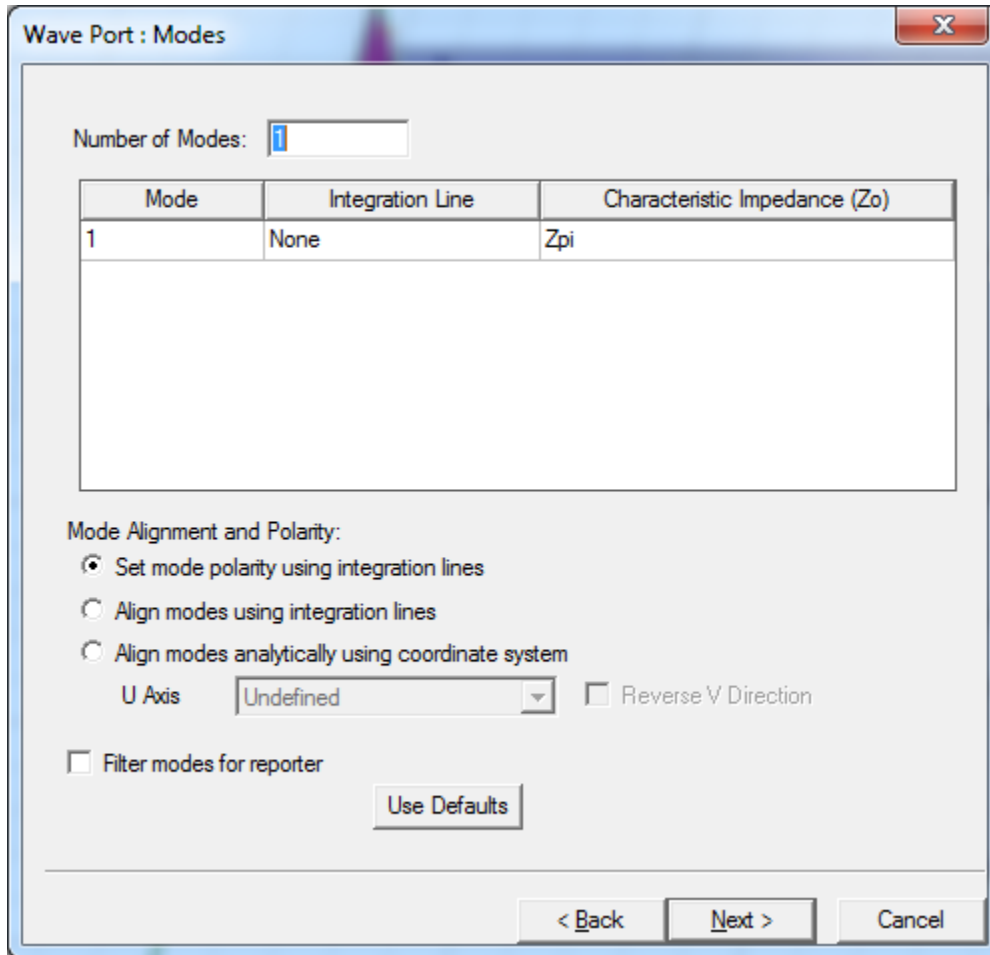


Figure 5-13: Wave port mode definition window.

To define the integration line, click the space under "Integration Line" where "None" is currently listed. Select "New Line..." and the window will change to a drawing mode with a green cursor. In the model draw a line on the port from the top of the signal line to the bottom of the ground plane at the center of the signal line width, using the point where the green cursor becomes a green triangle as a guide. After drawing the line, the port should look like Figure 5-14 below.

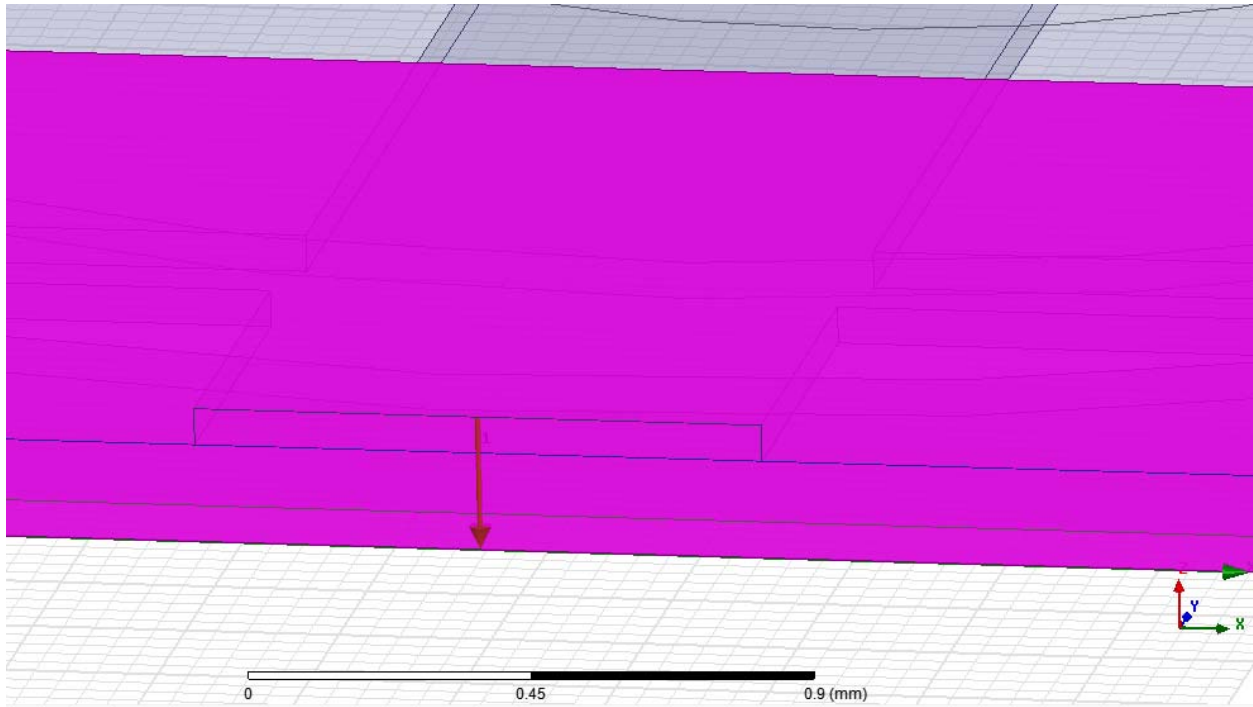


Figure 5-14: Integration line drawn from the signal line to the ground plane, represented by the red arrow.

In the next window, select "Renormalize All Modes" and select 50 ohm for the Full Port Impedance to match the ports to 50Ω. Repeat this process for the second port to define both excitation ports.

After setting the excitation ports, right-click Analysis in the Project Manager pane and click Add Solution Step. For this example, set the Solution Frequency to 4.2GHz and use a Maximum Number of Passes of 12 and a Maximum Delta S of 0.05. The solution frequency needs to be close to the resonant frequency of the device, so this step may require some iteration once a simulation is run to get an accurate solution. The maximum number of passes determines how many adaptive passes will be made to converge the solution, and the maximum delta S determines the allowed solution error.

Next, in the upper toolbar click the Add Frequency Sweep button that looks like a red line on a graph. This allows the user to define the parameters of the frequency sweep for the simulation.

For this example, select LinearCount for the Frequency Setup Type. Set the start frequency to 1 GHz and the stop frequency to 10GHz with a Count of 201. This will set 201 frequency points for the frequency sweep. Click OK.

Finally, right-click Results in the Project Manager Pane and click Create Modal Solution Data Report>Rectangular Plot. For this example, selection S Parameter for the category and S(1,1) and S(2,1) for the Y Trace variables. Click New Report to submit this change. To run the simulation, click the Analyze All button that looks like a green exclamation point in the top toolbar. Once the simulation is completed, the results should look similar to the frequency response shown in Figure 5-15 below.

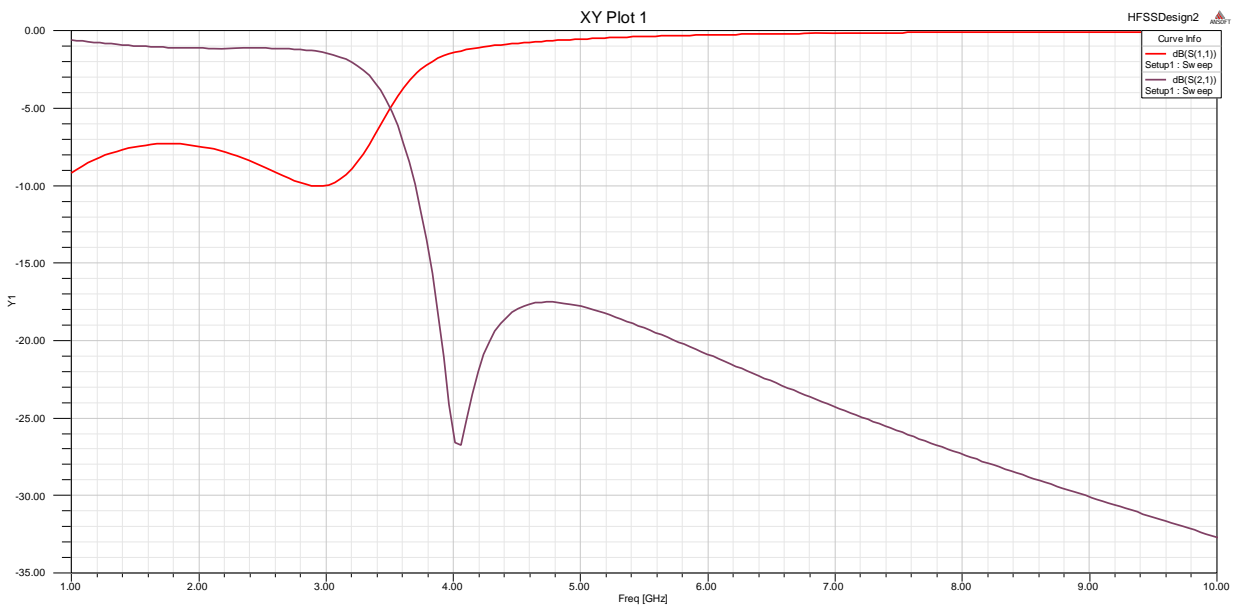


Figure 5-15: Simulation results for S11 and S21 of the example filter.

Chapter 6

Improved BPF Design

While metamaterial technology does make possible the creation of several types of compact filters with performance comparable or even superior to conventional designs, these devices are not without their challenges, especially the band-stop and band-pass versions. In particular, the frequency responses of metamaterial-loaded BSFs and BPFs may experience a sharp cutoff on the lower band due to the presence of a transmission zero, but these filters can be left with a smoothing effect in the upper band that results in an asymmetric frequency response [21] [30] [31]. An example of this upper band smoothing issue in the frequency response is shown below in Figure 6-1.

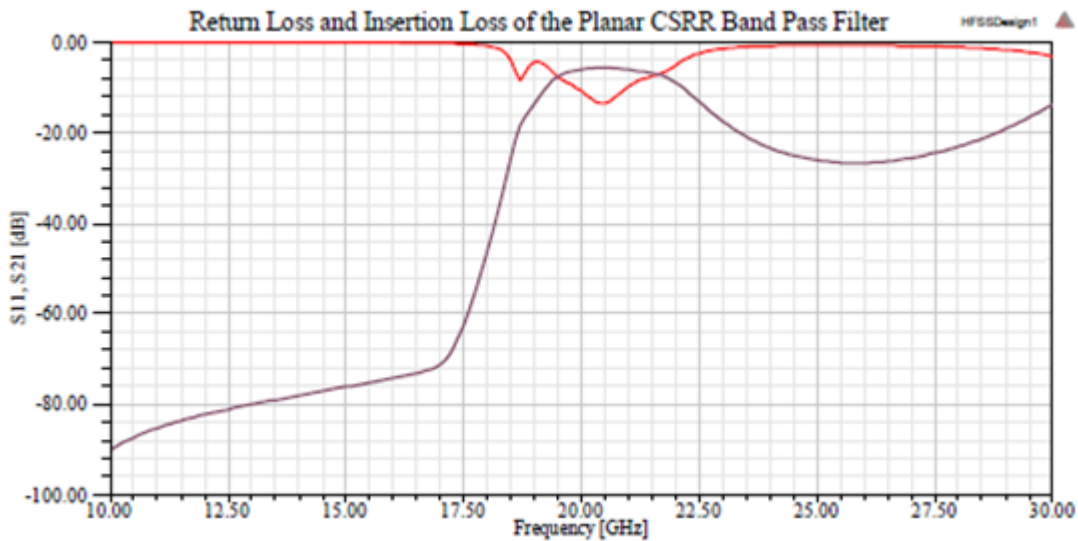


Figure 6-1: Frequency response of a metamaterial BPF. Red: Insertion loss (S11); Purple: Return loss (S21). [31]

This upper band issue can be a serious problem depending on the filter's application and expected environment, and this property is inherent to BSFs and BPFs must be considered during the filter design process.

In this work, an attempt has been made to mitigate this upper band smoothing problem in a CSRR-loaded BPF based on previous work at Auburn University [30] [31]. This was achieved by introducing a unique signal line design concept to the BPF that combines the shunt stub trait of the LPF with the series gap trait of the HPF, resulting in a single signal line element to act as a band-pass filter. Additional shunt inductance was added to increase the low-pass component of the filter and suppress the frequency response in the upper band in order to achieve symmetrical band-pass behavior. As with previous work, this filter was designed using an LCP substrate to realize a flexible filter for nonplanar surface applications. The design of this filter will be the focus of the rest of this chapter.

In [31], a planar band-pass filter using an LCP substrate was presented using periodic series capacitive gaps etched into the signal line. These gaps were placed at the center of the CSRR elements underneath the substrate and etched into the ground plane. The filter is shown below in Figure 6-2, and its frequency response is shown previously in Figure 6-1.

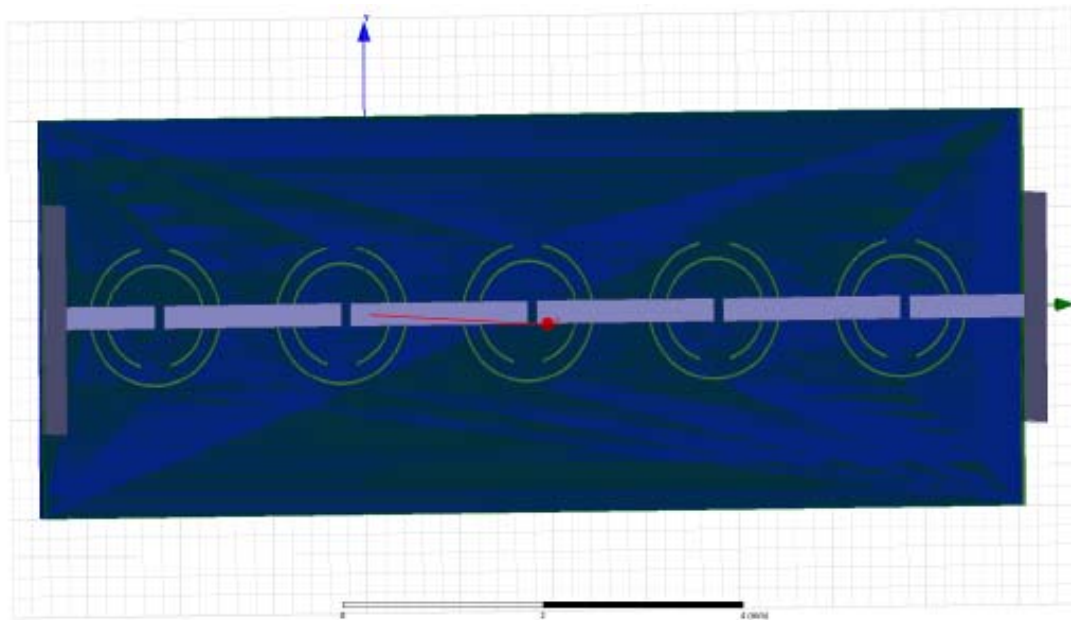


Figure 6-2: Metamaterial BPF using series etched capacitive gaps. [31]

To design a BPF with an improved upper band, a unit cell approach was taken. A unit cell design can be a simple starting point for the design of a higher order metamaterial filter due to the periodic nature of metamaterials. Cascading these unit cells, spaced apart an appropriate distance, will result in a filter that has behavior similar to, but better defined than, that of the unit cell. To design the unit cell, first a simple microstrip design was modeled in HFSS including the copper signal line, an LCP substrate and the copper ground plane. The basis for the new BPF is shown below in Figure 6-3.

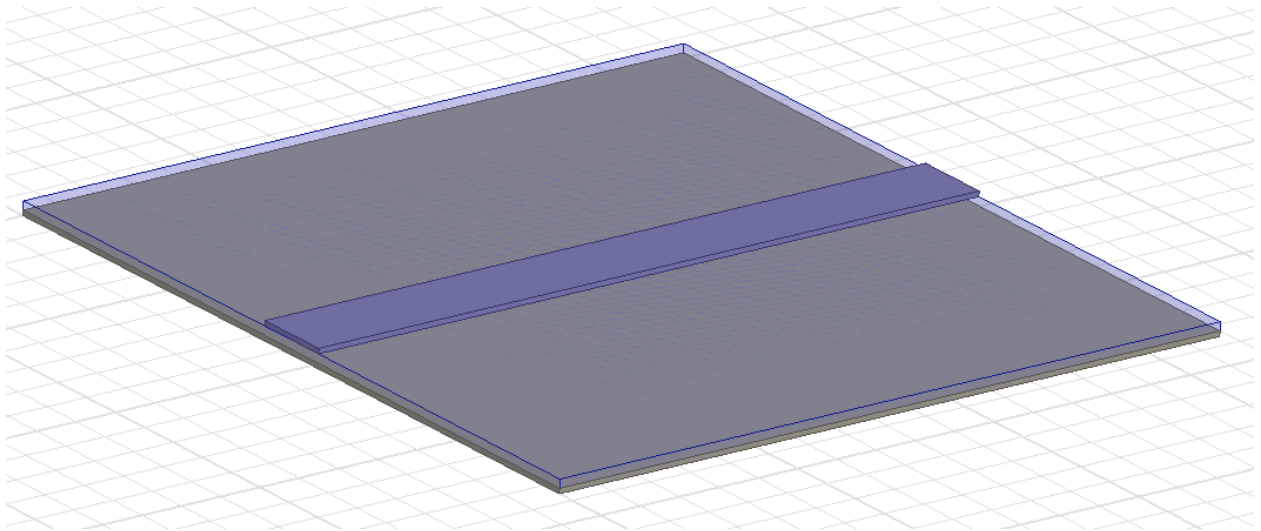


Figure 6-3: Simple microstrip design for the unit cell including the signal line, LCP substrate, and ground plane.

In the model, the signal line was matched to 50Ω using a transmission line calculator and has a width of 9.28mm, a height of $60.3\mu\text{m}$, and a length of 8.4mm. The LCP substrate is also 8.4mm long and has a width of 9.28mm and a height of 4 mil. Finally, the copper cladding that serves as the ground plane is 8.4mm in length, 9.28mm wide, and $60.3\mu\text{m}$ tall. The LCP substrate has a relative permittivity ϵ_r of 3.1, and the copper is defined as having a relative permeability μ_r of 0.999991.

Next, the CSRR rings were added to the ground plane. This was achieved by subtracting two concentric cylinders from the ground plane and using a small rectangle shape subtracted from the rings to create the ring gap. The filter model with the rings included is shown in Figure 6-4.

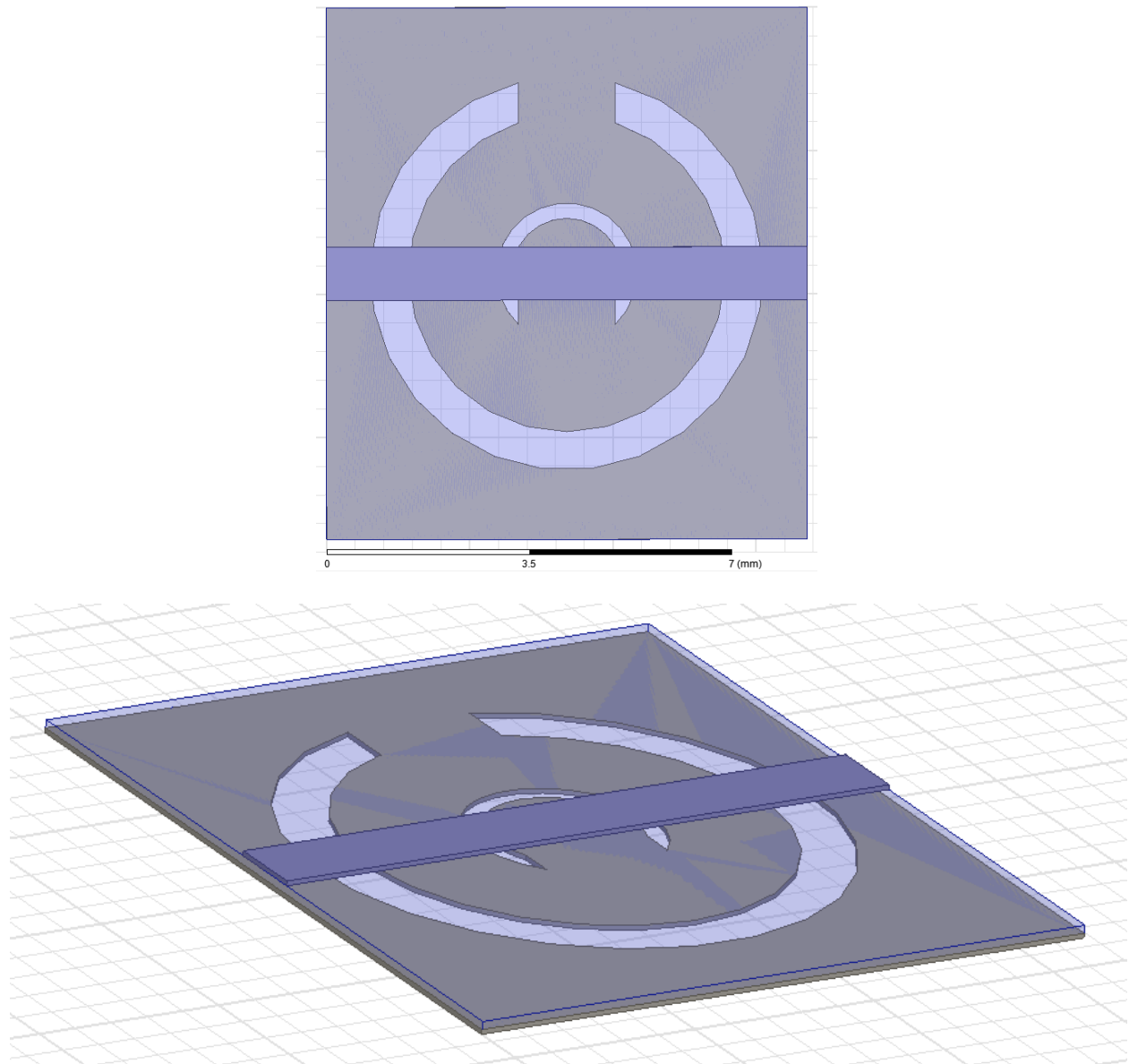


Figure 6-4: CSRR-loaded BPF model with CSRR rings etched into the ground plane.

In the model, the outer radius of the outer ring is 3.432mm, and the width of the outer ring is about 0.671mm. The outer radius of the inner ring is about 1.23mm, and the width of the inner ring is about 0.2685mm. The ring gaps are of equal length and are 1.6875mm long.

Next, the capacitive gap was added to the signal line. With this gap, the filter model now had the same elements as the BPF from the previous work. The filter with the added series gap is shown below in Figure 6-5.

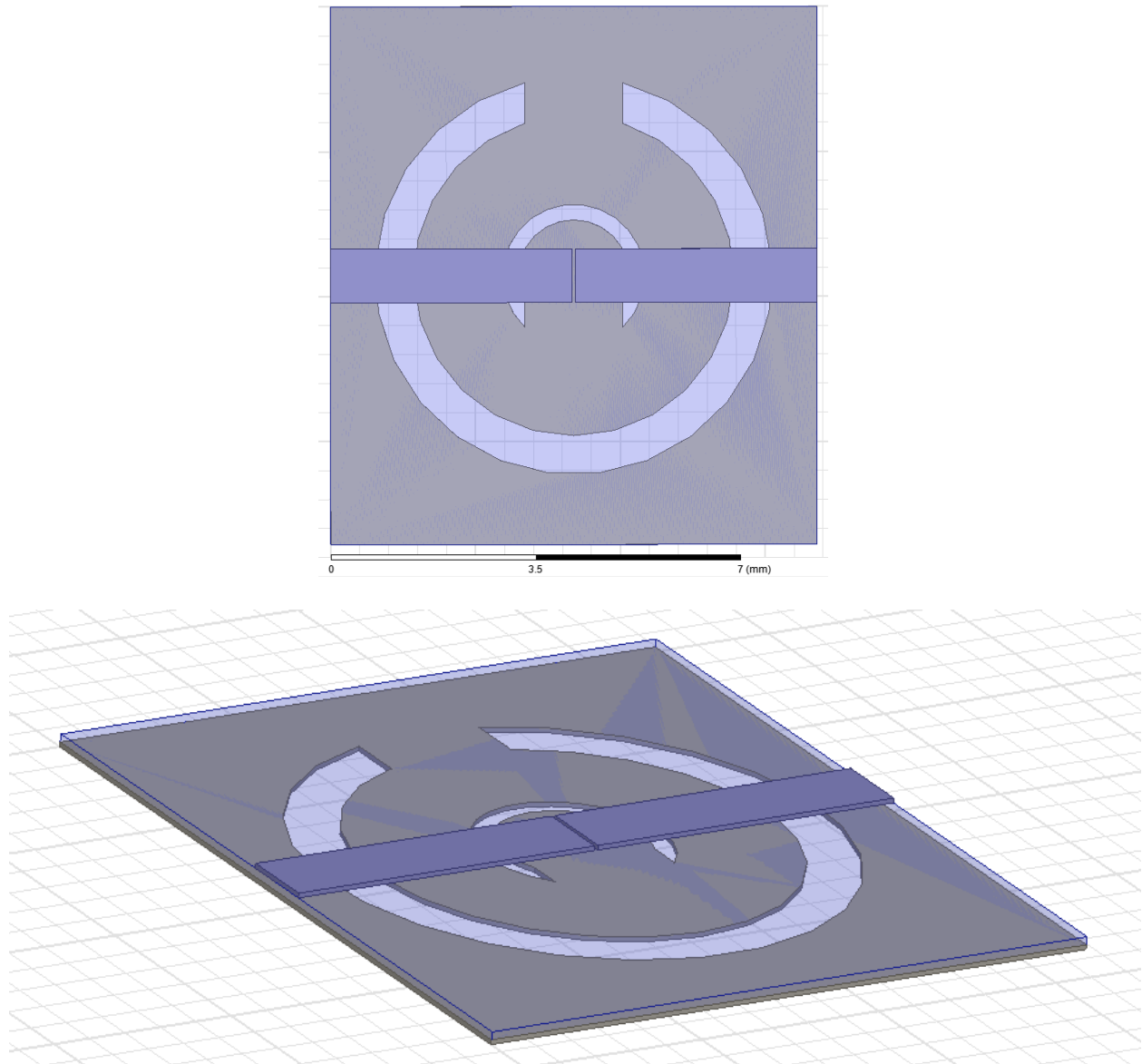


Figure 6-5: CSRR-loaded BPF design using only a series capacitive gap.

The series gap in this model is the same width as the signal line and is about $50\mu\text{m}$ in length. While this type of design has shown somewhat of a band-pass behavior, the frequency response in Figure 4-6 illustrates the problem with the upper band of this approach.

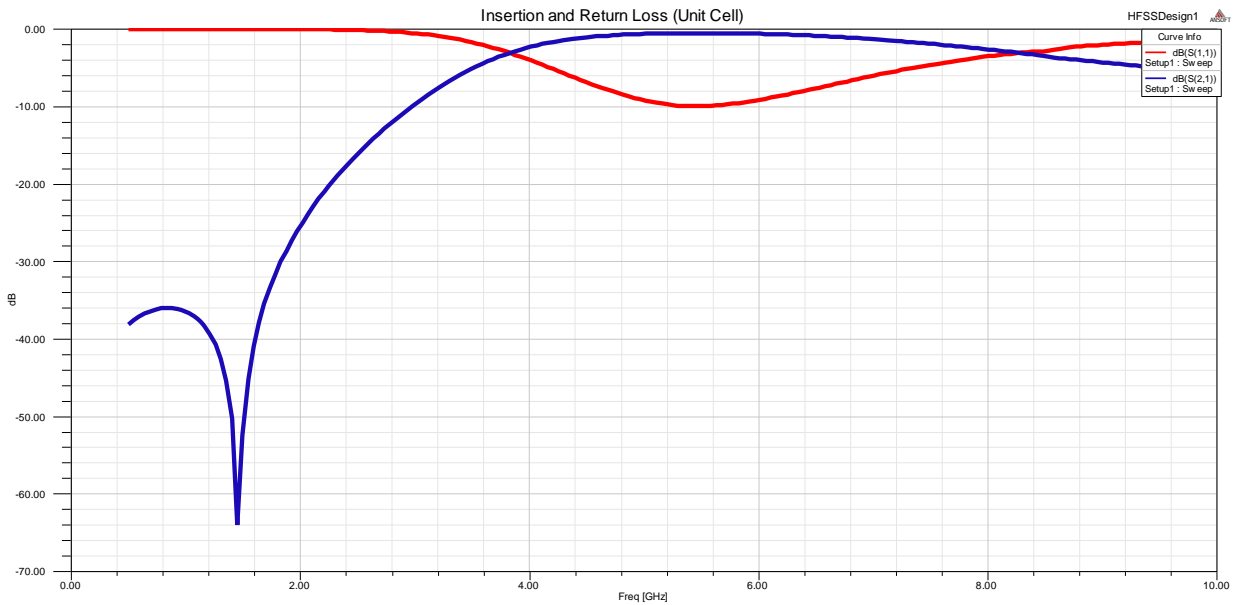
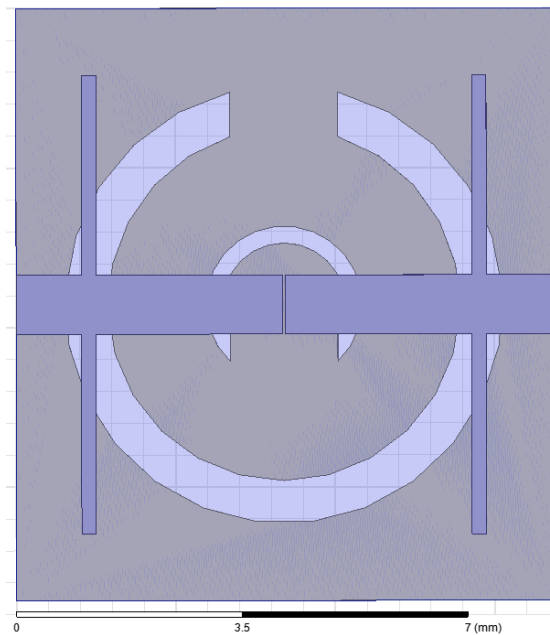


Figure 6-6: S11 (red) and S21 (blue) of the BPF using only a series gap.

In the figure, the insertion loss (S11) and return loss (S21) of the filter are simulated from 1GHz to 10GHz. Figure 6-6 shows that, without additional inductance on the signal line, the design acts like a combination of a HPF and a BPF. To generate a stronger low-pass response, shunt inductive line stubs were added to the signal line. The resulting filter is shown in Figure 6-7.



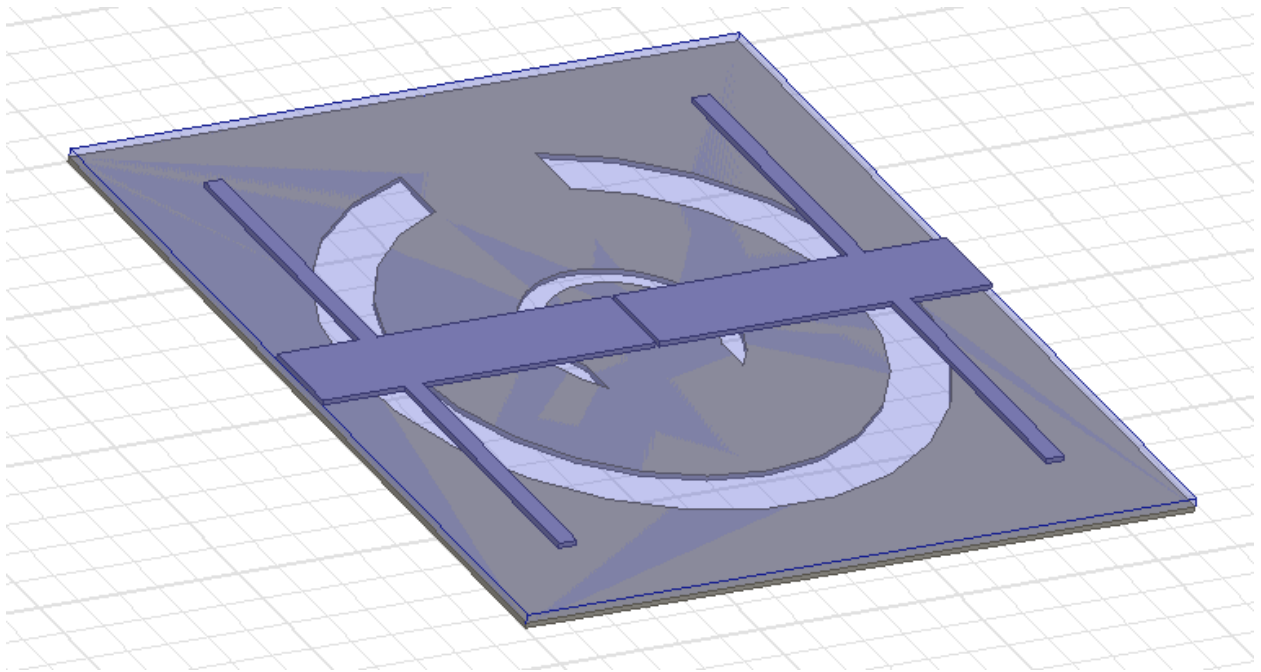


Figure 6-7: CSRR-loaded BPF design with series gap and shunt stubs.

In the model, the dimensions of the added shunt stubs are 7.19mm long and 225 μ m wide. While this addition does result in a better upper band response, some other problems arise. This is shown below in Figure 6-8.

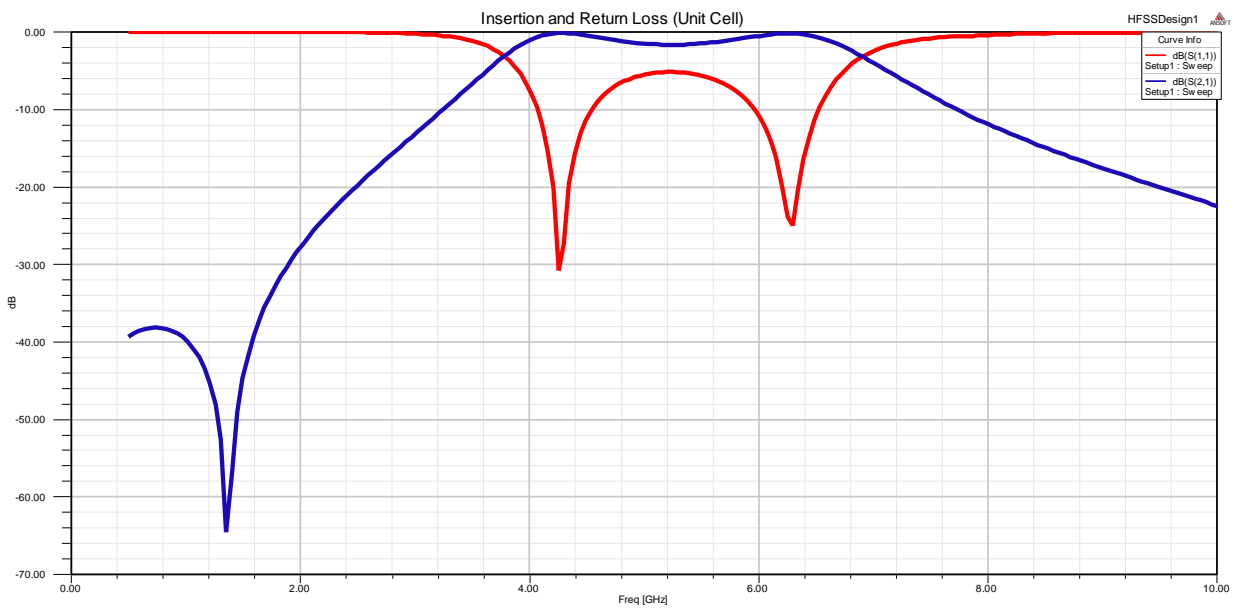


Figure 6-8: Frequency response of the CSRR-loaded BPF with series gap and shunt stubs.

In Figure 6-8, the filter does have a decreasing upper band, but it has developed a second resonance. To remove this second resonance, shunt stubs were added at the gap to filter out the higher resonant frequency. The combination low-pass/high-pass BPF is shown below in Figure 6-9.

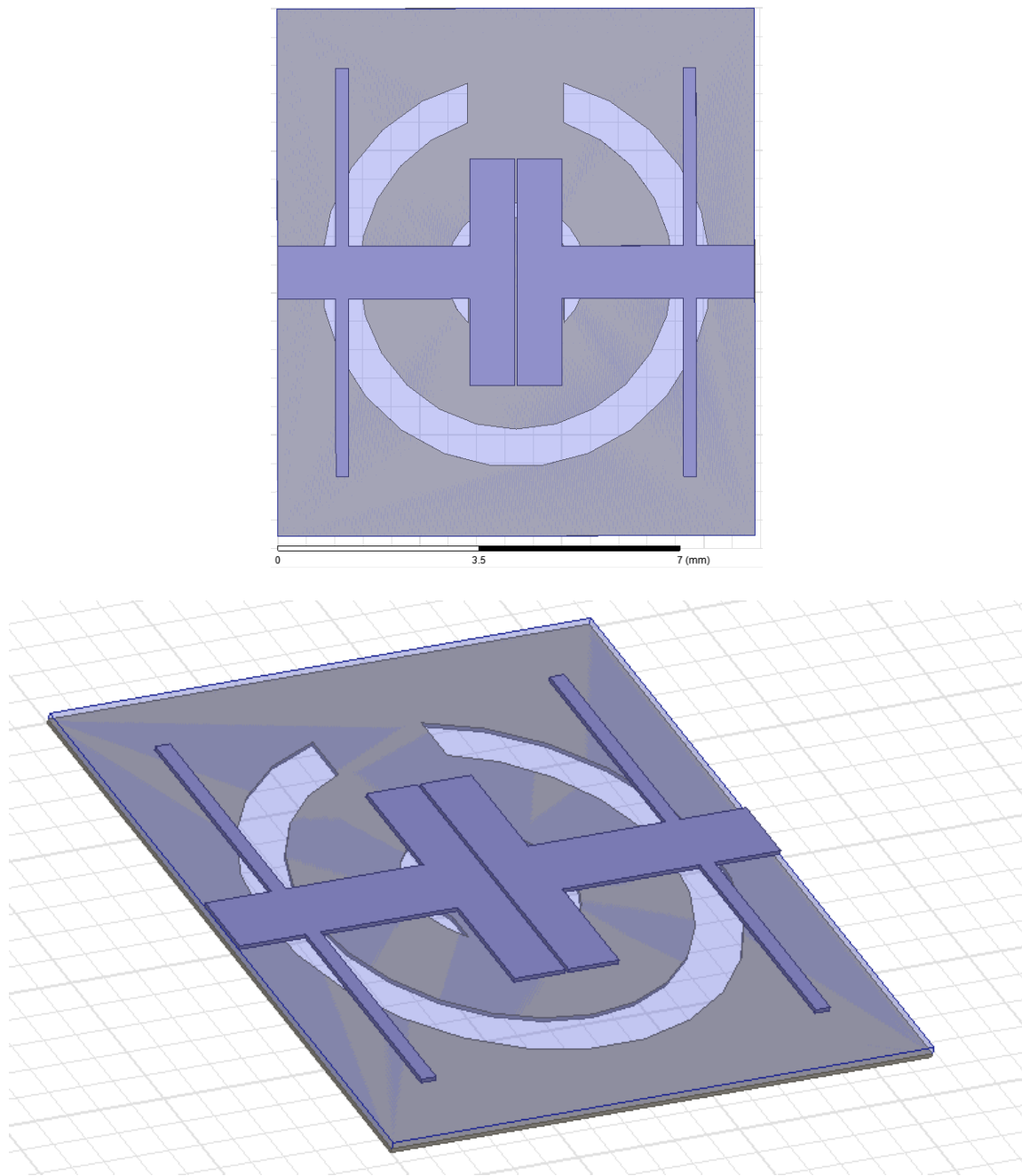


Figure 6-9: CSRR-loaded HPF with added high-pass characteristics.

In the model, the length of the newly added shunt stubs is 3.994mm, and the width of these stubs is 786.8 μ m. The frequency response of the filter with the added stubs is shown below in Figure 6-10.

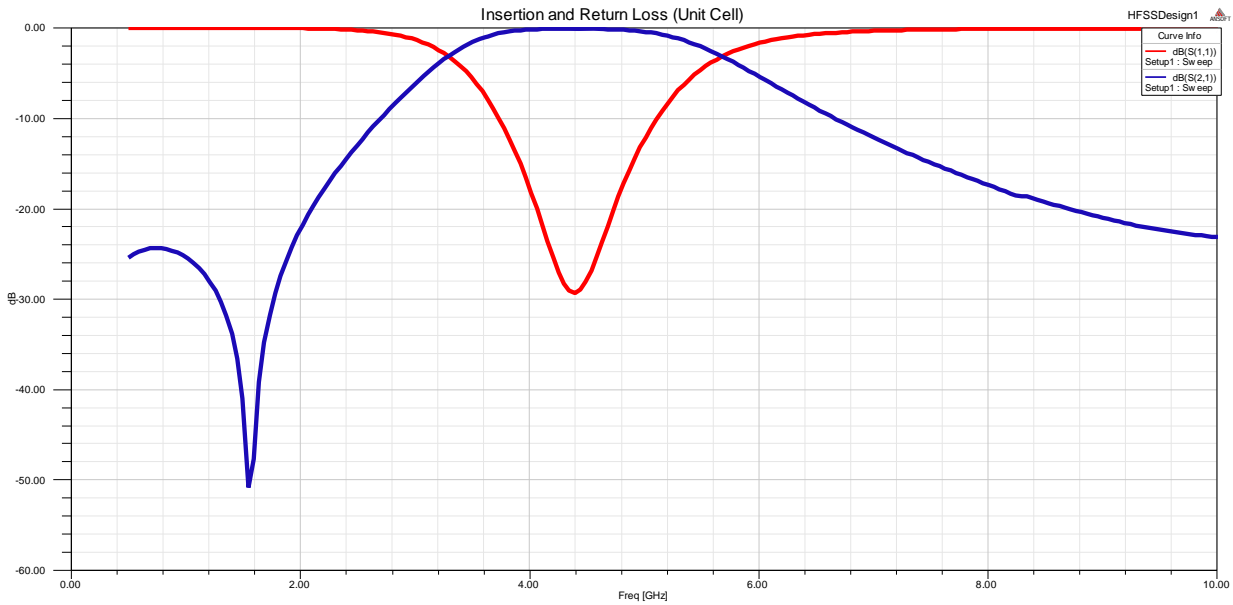


Figure 6-10: Frequency response of the BPF with series gap and all shunt stubs.

As is shown in Figure 6-10, the frequency response of the filter now looks similar to a standard band-pass filter. The filter exhibits a single passband with a single resonant frequency at 4.2GHz, and the 3db bandwidth is about 2.4GHz. At the resonant frequency, the S11 of the filter is about -30dB, and the S21 in the passband is close to 0dB. Most importantly, the upper band of the frequency response no longer curves upward, indicating an improvement in the upper band of the filter.

Chapter 7

Conclusion

Novel microwave filters made from transmission lines loaded with metamaterial structures called complementary split-ring resonators are easily realizable by adding these resonating rings to the ground plane of a microstrip line. At least four different types of filters are possible—low-pass, high-pass, band-stop, and band-pass filters. Band-stop and band-pass filters, however, experience a smoothing effect in the upper band of the frequency response that has a negative effect on filter performance. To correct this smoothing issue, the circuit models of the CSRR-loaded low-pass and high-pass filters have been examined in an attempt to improve a previous band-pass design.

By combining low-pass and high-pass concepts, a metamaterial band-pass filter has been designed using HFSS. While the previous design used high-pass concepts in the form of etched series capacitive gaps, shunt inductive stubs were not included originally. Adding shunt inductance to the signal line increases the low-pass component of the filter. As shown in the simulation results, this addition of shunt inductive stubs brought down the smoothed curve in the upper frequency band, resulting in a frequency response that shows better band-pass filter behavior. By designing the filter on LCP substrate, the fabrication of a high-order flexible band-pass filter that, based on previous work, would show little degradation in performance over a given radius of curvature is possible.

Chapter 8

Future Work

Having designed a unit cell of a CSRR-loaded band-pass filter, the next step in refining this design would be to expand this unit cell into a high-order filter by cascading several elements in series. This would sharpen the frequency response behavior of the filter. Additionally, the simulation results of this work could be verified by fabricating the design and testing a physical realization of the model. In the future, filters like the one presented in this work could be used in the design of advanced compact microwave filters and other microelectronic communication technology.

Bibliography

- [1] V. G. Veselago, "The electrodynamics of substances with simultaneously negative values of ϵ and μ ," *Sov. Phys. Usp.*, vol. 10, pp. 509-514, Jan-Feb 1968.
- [2] R. A. Shelby, D. R. Smith and S. Schultz, "Experimental verification of a negative index of refraction," *Science*, vol. 292, pp. 77-79, 6 April 2001.
- [3] J. B. Pendry, "Negative refraction makes a perfect lens," *Phys. Review. Lett.*, vol. 85, no. 18, pp. 3966-3969, October 2000.
- [4] Zani, M. Z. M.; Jusoh, M. H.; Sulaiman, A. A; Baba, N. H.; Awang, R. A.; Ain, M. F., "Circular patch antenna on metamaterial," in *International Conference on Electronic Devices, Systems, and Applications*, 2010.
- [5] W. Fei, H. Yu, Y. Shang, D. Cai and J. Ren, "A 96-GHz oscillator by high-Q differential transmission line loaded with complementary split-ring resonator in 65-nm CMOS," *IEEE Transactions on Circuits and Systems*, vol. 60, no. 3, pp. 127-131, March 2013.
- [6] A. K. Iyer and G. V. Eleftheriades, "Effective-medium properties of a free-space transmission-line metamaterial superlens," in *13th International Symposium on Antenna Technology and Applied Electromagnetics and the Canadian Radio Sciences Meeting*, 2009.
- [7] I. Zagoya-Mellado, A. Corona-Chavez and I. Llamas-Garro, "Miniaturized Metamaterial Filters Using Ring Resonators," in *International Microwave Workshop Series on Signal Integrity and High-Speed Interconnects*, Guadalajara, Mexico, 2009.
- [8] skullsinthestars, "Skulls in the Stars," 19 May 2009. [Online]. Available: <http://skullsinthestars.com/2009/05/19/what-does-negative-refraction-look-like/>. [Accessed February 2015].
- [9] J. B. Pendry, A. Holden, D. Robbins and W. Stewart, "Magnetism from conductors and enhanced nonlinear phenomena," *IEEE Trans MTT*, vol. 47, no. 11, pp. 2075-2083, November 1999.
- [10] J. B. Pendry, A. Holden, W. J. Stewart and I. Youngs, "Extremely low frequency plasmons in metallic meso structures," *Phys. Rev. Lett.*, vol. 76, pp. 4773-4776, 1996.
- [11] D. R. Smith, W. J. Padilla, D. C. Vier, S. C. Nemat-Nasser and S. Schultz, "Composite medium with simultaneously negative permeability permittivity," *Phys. Rev. Lett.*, vol. 84, no. 18, pp. 4184-4187, May 2000.
- [12] J. B. Pendry, "Metamaterials and the control of electromagnetic fields," 2007.
- [13] J. D. Baena, J. Bonache, F. Martín, R. M. Sillero, F. Falcone, T. Lopetegui, M. A. G. Laso, J. García-García, I. Gil, M. F. Portillo and M. Sorolla, "Equivalent-circuit models for split-ring resonators and complementary split-ring resonators coupled to planar transmission lines," *IEEE Trans. MTT*, vol. 53, no. 4, pp. 1451-1461, April 2005.
- [14] C. Saha, J. Y. Siddiqui and Y. M. M. Antar, "Square split ring resonator backed coplanar waveguide for filter applications," in *General Assembly and Scientific Symposium, 2011 XXXth URSI*, Istanbul, 2011.
- [15] P. Kaur, S. K. Aggarwal and A. De, "Double H shaped metamaterial embedded compact RMPA," in *2014 International Conference on Advances in Computing, Communications, and Informatics*, New Delhi, 2014.

- [16] C. Zhu, L. Li, H. Zhai, K. Li, Y. Chen, T. Li and C. Liang, "Multi-arm spiral metamaterial with electric and magnetic responses," in *2012 10th International Symposium on Antennas, Propagation & EM Theory*, Xian, 2012.
- [17] F. Falcone, T. Lopetegui, J. D. Baena, R. Marques, F. Martin and M. Sorolla, "Effective negative- ϵ stopband microstrip lines based on complementary split ring resonators," *IEEE Micr. Wireless Comp. Lett.*, vol. 14, no. 6, pp. 280-282, 7 June 2004.
- [18] F. Aznar, M. Gil, G. Siso, J. Bonache and F. Martin, "SRR- and CSRR-based metamaterial transmission lines: modeling and comparison," in *IEEE MTT-S International Microwave Workshop Series on Signal Integrity and High-Speed Interconnects*, Guadalajara, 2009.
- [19] F. Aznar, J. Bonache and F. Martin, "An improved circuit model for left-handed lines loaded with split ring resonators," *Appl. Phys. Lett.*, vol. 92, February 2008.
- [20] J. Bonache, M. Gil, O. Garcia-Abad and F. Martin, "Parametric analysis of microstrip lines loaded with complementary split ring resonators," *Microwave and Optical Tech. Lett.*, vol. 50, pp. 2093-2096, August 2008.
- [21] R. Marques, F. Martin and M. Sorolla, *Metamaterials with Negative Parameters*, Hoboken, New Jersey: John Wiley and Sons, Inc., 2008.
- [22] S. J. Orfanidis, *Electromagnetic Waves and Antennas*, Rutgers University, 2014.
- [23] H. K. Kwan, "Tunable bandpass passive digital filter design," in *2002 45th Midwest Symposium on Circuits and Systems*, 2002.
- [24] J. C. Hathaway and D. F. Babcock, "Survey of mechanical filters and their applications," in *Proceedings of the IRE*, 2007.
- [25] S. J. Park, C. P. I. Reines and G. M. Rebeiz, "High-Q RF-MEMS 4-6-GHz Tunable Evanescent-Mode Cavity Filter," *IEEE Trans. MTT*, vol. 58, no. 2, pp. 381-389, 26 January 2010.
- [26] T. H. Kim, W. K. Jeung, S. J. Yang, S. M. Choi, S. W. Park, H. H. Kim, J. Ha, M. J. Park, S. Kao, J. P. Hong, S. Yi, J. S. Hwang, J. H. Lim and W. B. Kim, "Miniaturization of optimization of RF SAW filter using wafer level packaging technology," in *57th Electronic Components and Technology Conference*, Reno, 2007.
- [27] D. Penunuri and K. M. Lakin, "RF filter design using LTCC and thin film BAW technology," in *2001 IEEE Ultrasonics Symposium*, Atlanta, 2001.
- [28] Umm Al-Qura University, [Online]. Available: <http://libback.uqu.edu.sa/hipres/Indu/indu14496.pdf>.
- [29] D. M. Pozar, *Microwave Engineering*, 4th ed., John Wiley and Sons, Inc., 2012.
- [30] J. Richard, "Metamaterial filters on LCP substrate using MEMS technology," 2011.
- [31] U. Blair, "Simulation and analysis of a metamaterial filter on a flexible liquid crystal polymer substrate," 2014.
- [32] Interplex Industries, Inc., "Advantages of using LCP based pre-molded leadframe packages for RF & MEMS applications," 14 December 2011. [Online]. Available: [http://www.interplex.com/interplex/resources/advantages-of-lcp-packages.pdf/\\$file/advantages-of-lcp-packages.pdf](http://www.interplex.com/interplex/resources/advantages-of-lcp-packages.pdf/$file/advantages-of-lcp-packages.pdf). [Accessed March 2015].
- [33] N. Kingsley, "Liquid crystal polymer: enabling next-generation conformal and multilayer electronics," *Microwave Journal*, pp. 188-200, 2008.

- [34] D. Gupta, P. Gupta, P. Chitransh and P. K. Singhal, "Design and analysis of low pass microwave filter using metamaterial ground structure," in *2014 International Conference on Signal Processing and Integrated Networks*, Noida, 2014.
- [35] P. Mondal, M. K. Mandal, A. Chaktabarty and S. Sanyal, "Compact bandpass filters with wide controllable fractional bandwidth," *IEEE Microwave and Wireless Comp. Lett.*, vol. 16, no. 10, pp. 540-542, 25 September 2006.
- [36] R. S. Kshetrimayum, S. Kallapudi and S. S. Karthikeyan, "Stopband characteristics for periodic patterns of CSRRs in the ground plane," *IETE Technical Review*, 2007.
- [37] S. Pasakawee, "Left-handed metamaterials realized by complementary split-ring resonators for RF and microwave circuit applications," 2012.